

1 SUPPLEMENTARY INFORMATION

2  
3 **A gravity-based three-dimensional compass in the mouse brain**

4  
5 Dora E Angelaki<sup>1,2</sup>, Julia Ng<sup>2</sup>, Amada M Abrego<sup>2</sup>, Henry X Cham<sup>2</sup>, Eftihia K Asproдини<sup>3</sup>, J David  
6 Dickman<sup>2,4</sup> and Jean Laurens<sup>2</sup>

7  
8 <sup>1</sup> Center for Neural Science and Tandon School of Engineering, New York University, NY, USA.

9 <sup>2</sup> Department of Neuroscience, Baylor college of Medicine, Houston, Texas, USA.

10 <sup>3</sup> Department of Pharmacology, Faculty of Medicine, School of Health Sciences, University of  
11 Thessaly, Larissa, Greece

12 <sup>4</sup> Department of Electrical and Computer Engineering, Rice University, Houston, Texas, USA.

13  
14 **Address for correspondence:**

15 Dr. Dora E. Angelaki

16 Email: [da93@nyu.edu](mailto:da93@nyu.edu)

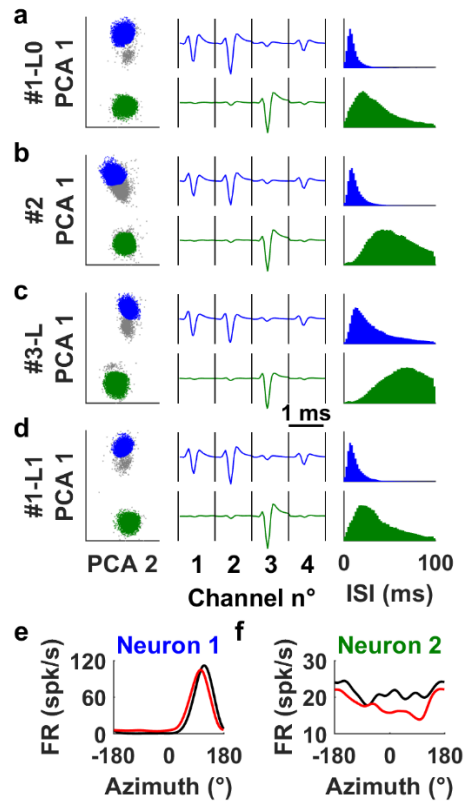
17 Center for Neural Science, Meyer 901

18 New York University, NY 10003

19

20

21

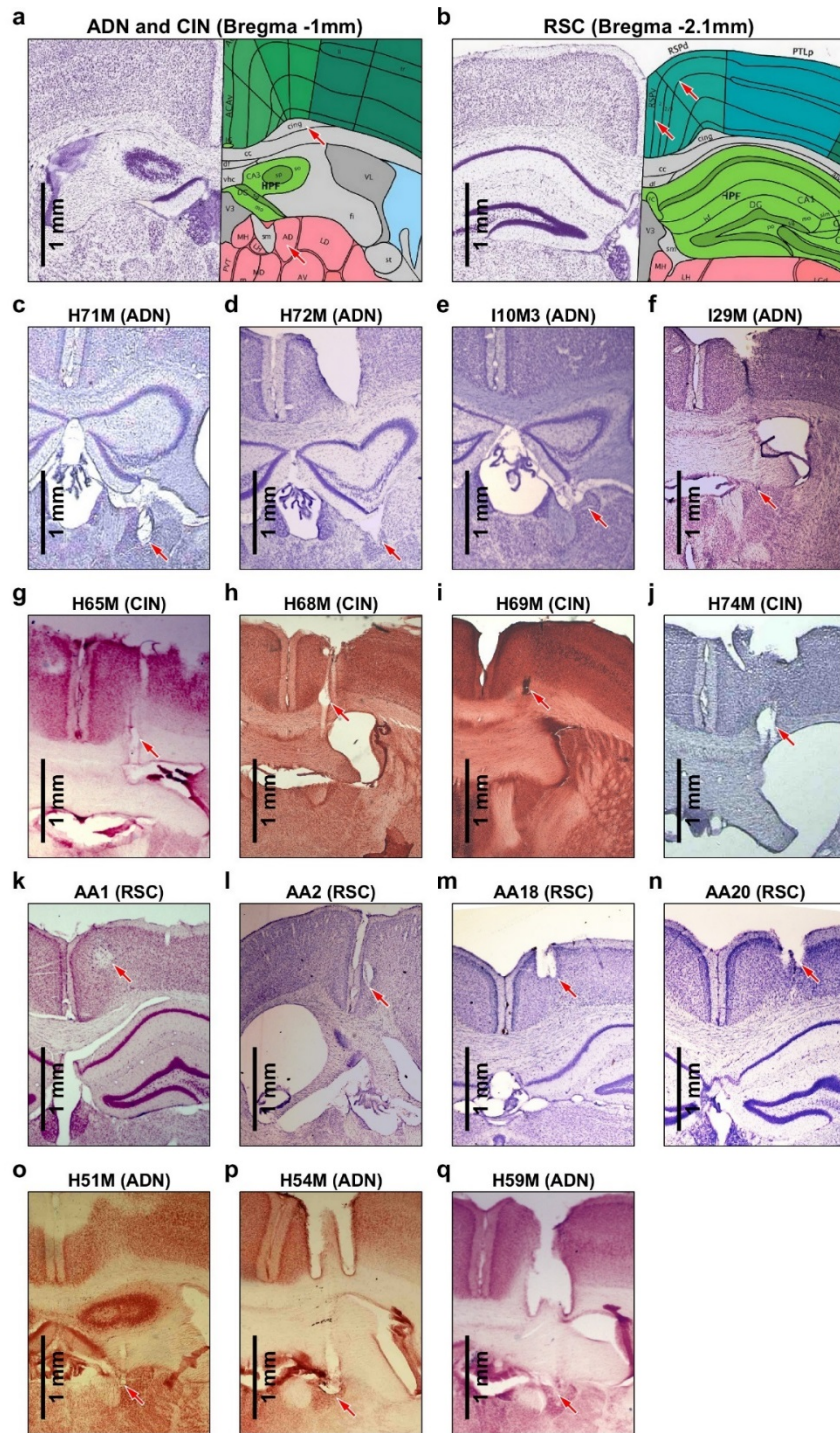


22

23 **Supplementary Figure 1: Recording stability across sessions.**

24 (a-d) Two neurons (color-coded in blue and green; animal H68M, CIN) were recorded  
 25 simultaneously during Experiment 1-L0 (a), Experiment 2 (b), Experiment 3-L (c) and Experiment  
 26 1-L1 (d). Left panels: spikes were extracted by manual clustering based on the maximum (peak)  
 27 and minimum (valley) voltage of the spikes, combined with factor analysis (the first two  
 28 components, PCA 1 and PCA 2, are shown here). When represented on a 2D plot, the spikes form  
 29 two clearly distinct clusters (blue and green). Grey dots represent unsorted events that result  
 30 from noise and background activity. Middle panels: average spike waveforms across all channels.  
 31 Right panels: the Inter-spike interval (ISI) histograms are conserved across Experiment 1-L0 and  
 32 1-L1 (a, d) but shift rightward during Experiment 2 (for neuron 2) and Experiment 3-L for both  
 33 neurons. This shift reflects the reduction of average firing rate during Experiments 2 and 3 due  
 34 to the general attenuation of neuronal firing in the rotator (see **Supplementary Fig. 8a,b**).

35 (e-f) Azimuth tuning curves of the neurons, recorded in the initial (black) and second (red)  
 36 freely moving session, i.e. before and after Experiments 2 and 3-L, are similar. This comparison  
 37 serves as confirmation of recoding stability across sessions (see also **Supplementary Fig. 3**).



38

39 **Supplementary Figure 2: Histological localization of neuronal recordings.**

40 (a,b) Annotated histology slides (image credit: Allen Institute<sup>1</sup>; available from  
 41 <http://atlas.brain-map.org/atlas?atlas=1&plate=100960268> and [http://atlas.brain-  
 map.org/atlas?atlas=1&plate=100960224](http://atlas.brain-<br/>
  42 map.org/atlas?atlas=1&plate=100960224)). The location of the sections relative to Bregma are

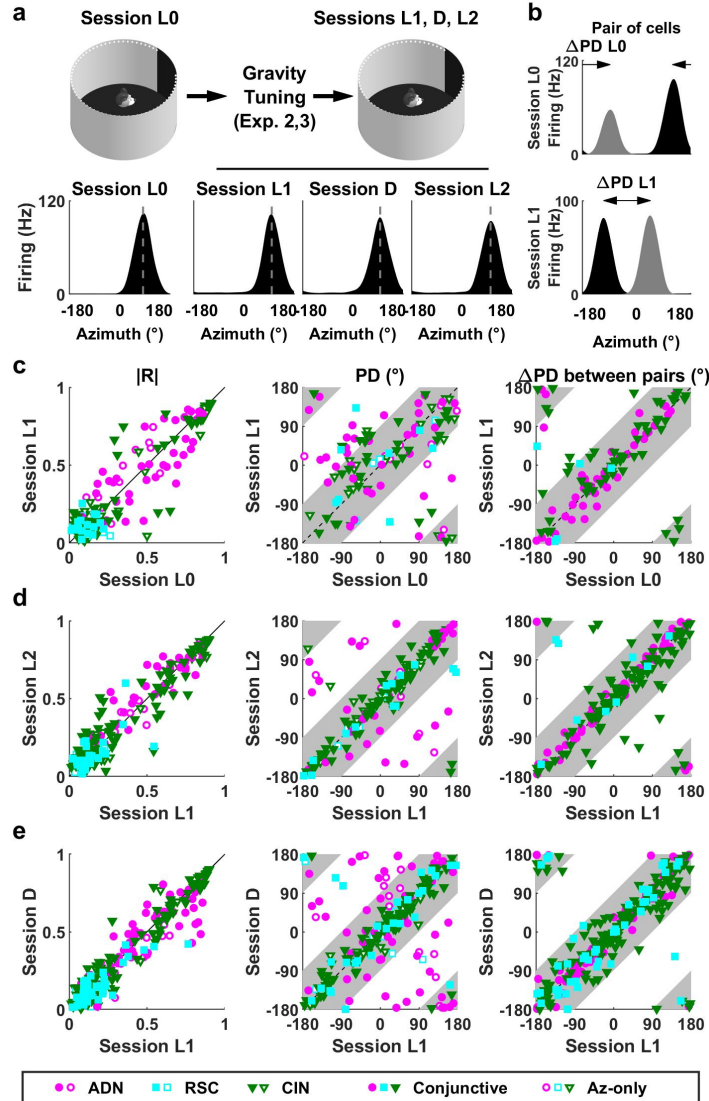
43 indicated in the title. Red arrows indicate the ADN (labelled “AD”), CIN (labelled “cing”) in (a), the  
44 I-II<sup>th</sup> layer of the granular RSC (labelled RSC<sub>v</sub>; left arrow) and the V<sup>th</sup> layer of the dysgranular RSC  
45 (RSC<sub>d</sub>; right arrow) in (b). Note that the ADN extends from Bregma -0.4mm to Bregma -1.1mm.  
46 Nissl-stained sections of all animals included in this study are shown; tetrode tracks are indicated  
47 by arrows.

48 **(c-f)** Recordings in the ADN. In all animals, the ADN appears as a characteristic triangular-  
49 shaped and densely stained nucleus. In H71M, H72M and I10M3, the ADN appears below the  
50 hippocampus, i.e. more caudal than usually indicated in brain atlases<sup>1,2</sup>. However, we confirmed  
51 that the nucleus marked by an arrow is indeed the ADN in each mouse by examining all  
52 microscopic sections and locating the anterior extremity of the thalamus as well as the anterior  
53 and posterior extent of the ADN.

54 **(g-j)** Recordings in the cingulum fiber bundle.

55 **(k-n)** Recordings in the RSC (AA1; AA18; AA20: dysgranular RSC; AA2: granular RSC; layer  
56 indeterminate).

57 **(o-q)** Additional recordings in the ADN. These animals were used in preliminary  
58 experiments where the rotator contained limited visual cues, precluding the measurement of  
59 azimuth tuning in the rotator. These animals are included only in **Supplementary Fig. 18**.



60

61 **Supplementary Figure 3: Response of Azimuth-tuned cells during unrestrained motion.** As  
 62 summarized in this analysis, azimuth-tuned cells conform to well-established properties<sup>3,4</sup>.

63 (a) Illustration of the sequence of recordings and example cell. At the beginning of an  
 64 experimental day, azimuth tuning is recorded in light as the mouse forages freely in a circular  
 65 arena (session L0). The mouse is then transferred to the platform and rotator to characterize its  
 66 3D tuning (Exp. 2-3; see **Supplementary Table 2** and **Methods**), upon completion it is returned  
 67 to the freely moving arena and azimuth tuning is measured in light again (session L1), then in  
 68 darkness (D), then again in light (L2). An example azimuth-tuned cell with stable preferred  
 69 direction (PD) in all sessions in the arena (L0, L1, D, L2).

70           **(b)** Two simultaneously recorded cells (grey and black tuning curves) that changed PDs  
71 between sessions L0 and L1 (see also other mouse studies<sup>5</sup>). Importantly, both cells shift  
72 together, such that the difference angle between their PD ( $\Delta$ PD) remains constant. Thus,  
73 comparing  $\Delta$ PD across cell pairs allows testing whether azimuth-tuned cells form a coherent  
74 neuronal compass even when this compass drifts from one session to another.

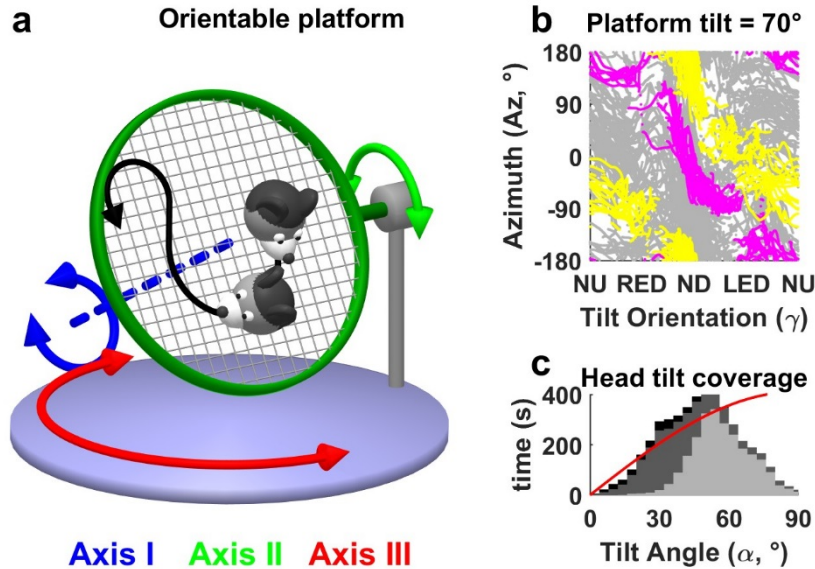
75           **(c)** Azimuth response stability between sessions L0 and L1. Left: There is no significant  
76 difference in tuning strength (Mean vector length  $|R|$ : signed rank tests,  $p > 0.5$  for all groups;  
77 Bonferroni correction applied; data from all cells significantly tuned to azimuth in at least one  
78 session;  $n = 54$  ADN; 33 RSC; 83 CIN). Middle: Comparison between the PD of individual cells.  
79 Only HD cells significantly tuned ( $p < 0.01$ ) in both sessions are included. PDs of a small  
80 subpopulation may drift between session L0 and L1 (PD shift  $> 90^\circ$  in 14/46 ADN; 3/12 RSC; 7/56  
81 CIN cells, i.e. 21% cells total). Grey bands represent sectors where the PDs shift by less than  $90^\circ$ .  
82 Right:  $\Delta$ PD between pairs of simultaneously recorded cells. Only cells significantly tuned ( $p < 0.01$ )  
83 in both sessions are included. PD differences are stable ( $< 90^\circ$  shift) in 93% (45/46 ADN; 4/5 RSC;  
84 50/55 CIN) of cells pairs. Thus, although PD may shift between L0 and L1, the PD of all cells tend  
85 to shift together, in line with predictions of an attractor network<sup>4</sup>.

86           **(d)** Azimuth response stability between sessions L1 and L2 (same legend as in c). There is  
87 no significant difference in tuning strength ( $p = 0.08$  for ADN,  $p > 0.5$  for other groups;  $n = 55$  ADN;  
88 39 RSC; 135 CIN). Only 11% of cells (15/48 ADN; 2/19 RSC; 1/92 CIN) drift more than  $90^\circ$ . PD  
89 differences are stable ( $< 90^\circ$  shift) in 96% (61/61 ADN; 7/9 RSC; 102/108 CIN) of cell pairs. Thus,  
90 PD are more stable between L1 and L2 compared to L0 and L1, likely because of the shorter time  
91 interval between L1 and L2 and/or the use of 3D stimuli in-between sessions L0 and L1.

92           **(e)** Azimuth response stability between sessions L1 and D (same legend as in c,d). Tuning  
93 strength is slightly attenuated in darkness in RSC (linear regression slope=0.74,  $p < 10^{-4}$ ;  $n = 81$ )  
94 but not in other areas (ADN:  $n = 70$ ,  $p = 0.14$ ; CIN:  $n = 143$ ;  $p = 0.3$ ). Only 13% (25/63 ADN; 4/44  
95 RSC; 0/113 CIN) of PDs drift more than  $90^\circ$ . PD differences are stable ( $< 90^\circ$  shift) in 99% (84/84  
96 ADN; 45/46 RSC; 146/148 CIN) of cell pairs.

97





98

99 **Supplementary Figure 4: Freely moving protocol for measuring 3D tuning in unrestrained, mice.**

100 (a) Illustration of the 3D orientable platform setup: mice walk freely (black arrow) on a  
 101 meshed platform that can rotate around 3 axes (blue, green, red). Walking on the platform  
 102 changes tilt orientation ( $\gamma$ ; see **Supplementary Fig. 5**) and azimuth simultaneously. Rotating the  
 103 base (Axis III) changes azimuth but not tilt orientation. Axis II is used to change tilt angle ( $\alpha$ ; see  
 104 **Supplementary Fig. 5**). Recordings are performed in 5-8-minute blocks where mice walk freely  
 105 while axis II-III are set to a static position. Axis I is repositioned within each block, as explained  
 106 below.

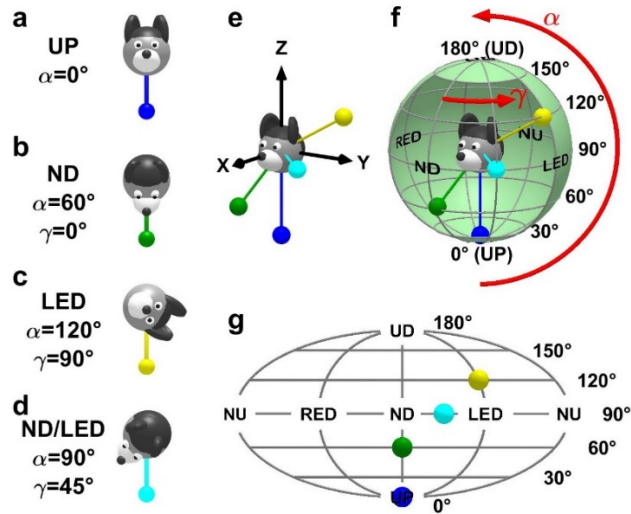
107 (b) Distribution of azimuth (Az) and tilt orientation (angle  $\gamma$ ) in eight 5-min blocks where  
 108 the platform was tilted  $70^\circ$  (average head tilt =  $60 \pm 15^\circ$ , as mice tend to partially compensate with  
 109 their head). Yellow, magenta: data recorded during two 5-min blocks corresponding to different  
 110 configurations (same tilt angle, but different positions of Axis III). Azimuth and tilt orientation  
 111 vary together as animals walk within one block, but azimuth is offset when Axis III is rotated  
 112 between blocks, thus allowing to scan the entire tilt orientation/azimuth plane.

113 (c) Distribution of head tilt angle ( $\alpha$ ) in the same recording session (black/grey/light grey:  
 114 data collected with the mesh tilted  $0^\circ$ ,  $45^\circ$ ,  $70^\circ$ , respectively). Red curve: distribution required for  
 115 uniform sampling of tilt orientation, illustrating relatively uniform sampling up to  $\sim 60^\circ$ ). Note  
 116 that, if only Axis III was rotated to change azimuth between blocks, the same physical portions of  
 117 the platform would always be oriented downward (or upward, or horizontally). In this situation,

118 local orientation on the platform itself would correlate with tilt relative to vertical. This could  
119 create a confounding factor since azimuth-tuned cells may potentially be referenced to the  
120 platform itself instead of distal cues<sup>6</sup>. To eliminate this confound, we rotated Axis I randomly in  
121 the middle of each block. Because of this added complexity, earth-horizontal azimuth tuning in  
122 **Fig. 2a** was evaluated based on data recorded in the arena.

123





124

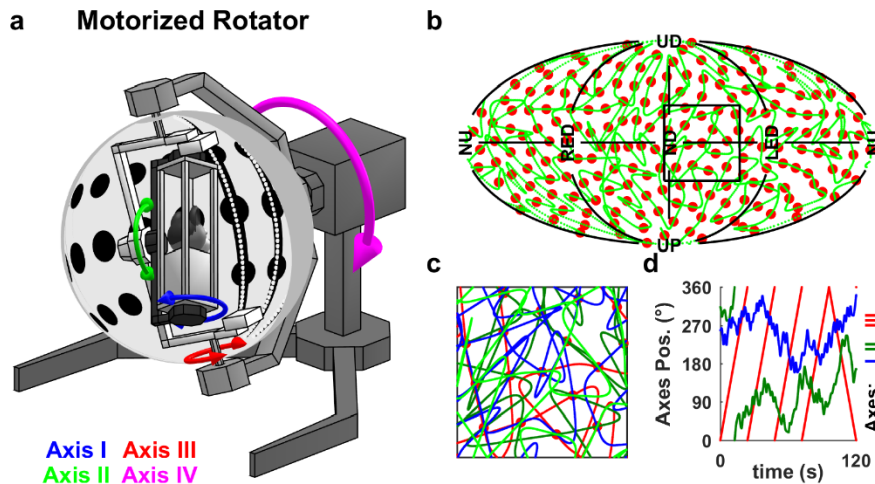
125 **Supplementary Figure 5: Coordinate systems for tilt relative to vertical.** A convenient way to  
 126 express head orientation to vertical is to represent the orientation of an allocentric vertical vector  
 127 in egocentric coordinates. In this study, we chose a downward-pointing vertical vector as a  
 128 reference. We generally refer to this vector as the gravity vector **G** for simplicity, although the  
 129 approach can be applied to any other vertical reference. This vector is encoded in 3D Cartesian  
 130 coordinates for data analysis and modeling purposes. However, since its length is constant, it is  
 131 restricted to a 2D sphere surrounding the head. Therefore, we use a simpler spherical coordinate  
 132 system to describe head tilt and represent tilt tuning curves.

133 **(a-d)** Four example tilt orientations, expressed in a spherical coordinate system ( $\alpha$ ,  $\gamma$ )  
 134 where  $\alpha$  is the tilt angle and  $\gamma$  is tilt orientation:  $\gamma = 0^\circ$  and  $\gamma = 180^\circ$  correspond to nose-down  
 135 (ND) and nose-up (NU) tilt;  $\gamma = 90^\circ$  and  $\gamma = -90^\circ$  correspond to left-ear-down (LED) and right-ear-  
 136 down (RED) tilt. The colored pendulum/ball represents the gravity vector.

137 **(e)** Representation of the gravity vector in (a-d) in egocentric Cartesian coordinates.

138 **(f)** Spherical topology of tilt orientation. When head tilt spans all possible orientations,  
 139 the tip of the gravity vector spans a sphere surrounding the head. The tilt variable  $\alpha$  corresponds  
 140 to the latitude on the sphere. Upright (UP,  $\alpha=0^\circ$ ) and upside-down (UD,  $\alpha=180^\circ$ ) orientations  
 141 correspond to the lower and upper pole respectively. The orientation variable  $\gamma$  corresponds to  
 142 the longitude.  $90^\circ$  tilt in ND, LED, NU and RED orientations are marked.

143 **(g)** Planar representation of the sphere using an equal-area Mollweide projection. The 4  
 144 tilt orientations in (a-d) are marked with color balls.



145

146 **Supplementary Figure 6: Rotator and protocol for measuring 3D tuning in restrained mice.**

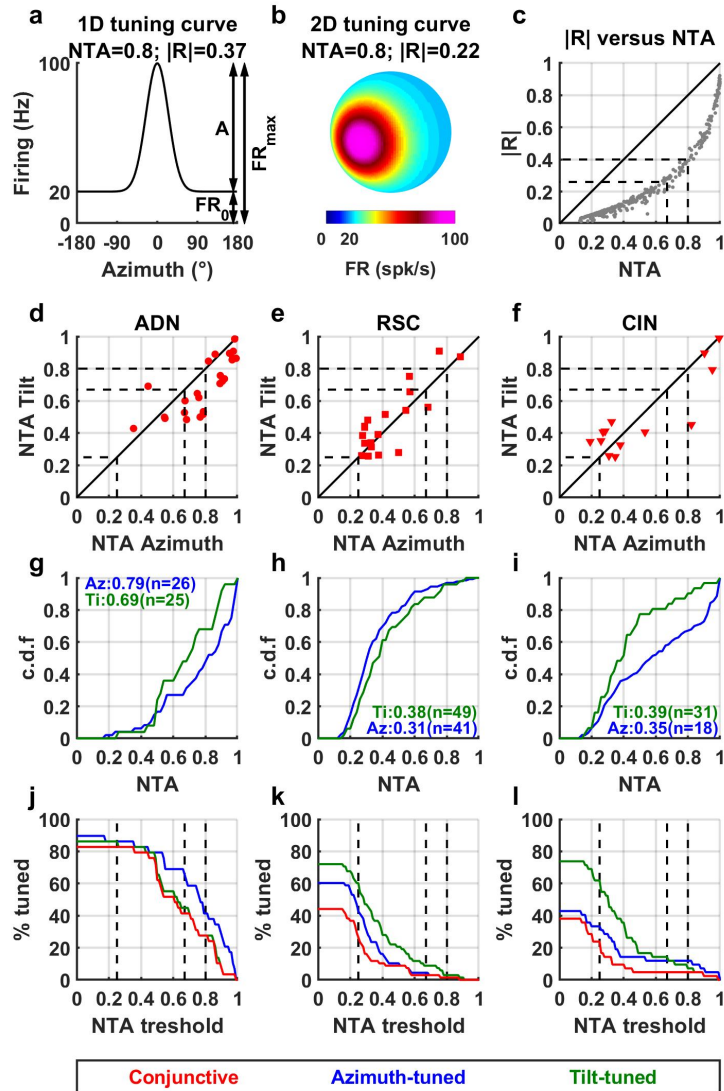
147 **(a)** Illustration of the motorized rotator; the 4-rotation axes are indicated by colored  
 148 arrows.

149 **(b)** Pseudo-random trajectory (green curve) used to measure tilt tuning. The trajectory  
 150 visits 200 uniformly distributed tilt positions (red dots). The full protocol scans the entire tilt  
 151 space 8 times by running through 4 distinct trajectories, each of which is ran twice in opposite  
 152 directions.

153 **(c)** Detail of the highlighted square in (b), with 4 distinct trajectories.

154 **(d)** Position of the rotator's 3 inner axes during a 2 min segment of the motion. Axes I  
 155 (inner yaw, blue) and II (middle, pitch/roll, green) are used to manipulate 2D head tilt relative to  
 156 vertical, while axis III (outer yaw, red) is used to continuously vary azimuth. Axis IV is used to tilt  
 157 the setup in Experiment 3-T (**Supplementary Table 1**).

158



159

160 **Supplementary Figure 7: Tuning strength in tilt- and azimuth-tuned cells.**

161 **(a)** We define a measure of tuning strength called normalized tuning amplitude (NTA),  
 162 illustrated here for a 1D tuning curve. We decompose firing rate into a baseline firing  $FR_0$  and a  
 163 modulation amplitude  $A$ . The peak firing rate is  $FR_{max}=FR_0+A$ . Normalized tuning amplitude is  
 164 defined as  $NTA=A/FR_{max}$ . The normalized tuning amplitude of this example is  $NTA = 0.8$ ; and the  
 165 mean vector length is  $|R|=0.37$ .

166 **(b)** Illustration of a 2D tuning curve on a sphere, used to model tilt tuning. This distribution  
 167 has identical baseline, amplitude and standard deviation as in (a) and therefore, the normalized  
 168 tuning amplitude is also  $NTA = 0.8$ . However, the mean vector length is  $|R|=0.22$ ; i.e. lower than  
 169 in (a). This is because the area of baseline firing on a sphere (cyan in b) amounts to a larger portion

170 of the tuning curve than in a 1D tuning curve, resulting in a lower  $|R|$  value. Therefore, the mean  
171 vector length is inappropriate for comparing azimuth (1D) and tilt (2D) tuning. Furthermore, the  
172 mean vector would be even lower in double-peaked curves, where the second peak would bring  
173 the mean vector even closer to zero. Finally, the mean vector is disproportionately influenced by  
174 a cell's baseline firing rate even in 1D, for instance  $|R|$  in panel (a) would increase from 0.37 to  
175 0.91 if the cell's baseline firing was set to 0. These limitations motivated us to develop the NTA  
176 measure.

177 **(c)** Comparison of the mean vector length ( $|R|$ ) and normalized tuning amplitude for  
178 azimuth tuning in Experiment 1-L (**Supplementary Table 2**; data from all significantly-tuned cells).  
179 Although the scaling between the two measures is non-linear, there is a clear relationship  
180 between them, indicating that they provide the same information. Therefore, the normalized  
181 tuning amplitude is as suitable as the mean vector for quantifying tuning strength, with the  
182 advantage that it allows for a fair comparison between 1D and 2D tuning curves.

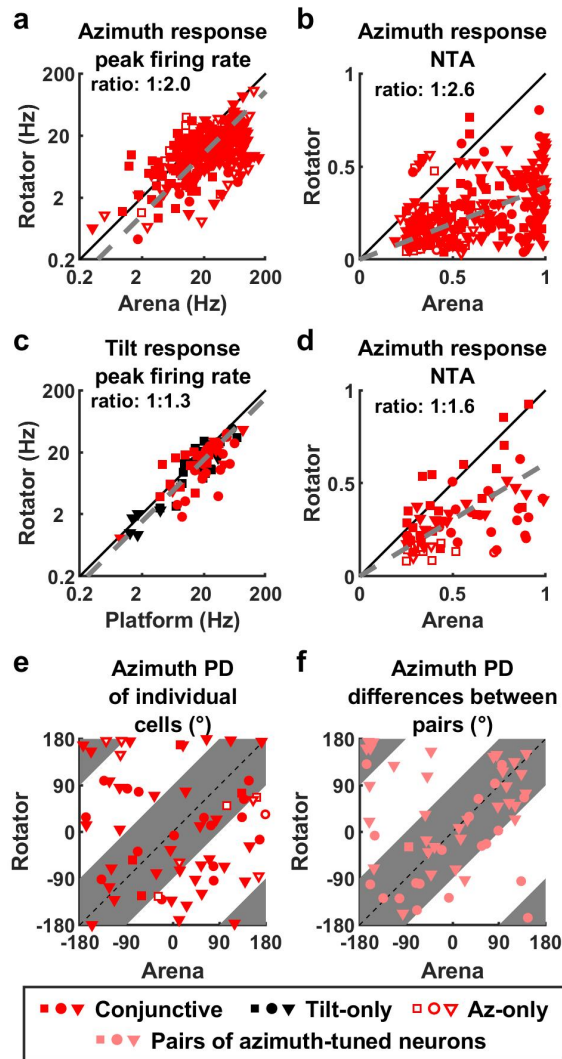
183 **(d-f)** Comparison of the normalized tuning amplitude of azimuth and tilt tuning for all  
184 conjunctive cells (as in **Fig. 2a**). Previous studies<sup>5,7</sup> have classified neurons as HD cells when  
185  $|R|>0.26$  or  $|R|>0.4$ . We infer from the population response in (c) that these values correspond  
186 to  $\text{NTA}\approx 0.67$  and  $\text{NTA}\approx 0.8$ , respectively. In the present study, we classified cells as azimuth or tilt-  
187 tuned using statistical criteria: if tuning passed a shuffling test (at  $p<0.01$ ), as long as  $\text{NTA}>0.25$   
188 (to exclude low-modulating cells). The three thresholds ( $\text{NTA}=0.25, 0.67, 0.8$ ) are indicated by  
189 vertical dashed lines. Although the statistical criterion we used was more inclusive compared to  
190 the fixed threshold of previous studies, the 3D tuning properties described here are found in  
191 those cells that pass the more restrictive criteria of previous studies, as detailed in subsequent  
192 panels.

193 **(g-i)** Cumulative distribution of NTA for all azimuth-tuned (blue) and tilt-tuned (green)  
194 cells that passed the shuffling test (not only conjunctive cells as in panels d-f). Median values of  
195 NTA and number of cells are indicated in the panels. The median values of tilt and azimuth tuning  
196 are comparable in all regions.

197 **(j-l)** Percentage of cells that would be classified as azimuth-tuned (blue), tilt-tuned (green)  
198 and conjunctive (red) by passing the shuffling test ( $p<0.01$ ) and exceeding a variable NTA

199 threshold, expressed as a function of that threshold, but including all recorded cells in both the  
200 arena and platform setups. Note that the threshold value of  $NTA = 0.25$  used in the present study  
201 allows for a large fraction of cells to be classified as azimuth-tuned, tilt-tuned or conjunctive (e.g.  
202 86% azimuth-tuned and 86% tilt-tuned in ADN). Using a more stringent threshold (e.g.  $NTA = 0.8$ )  
203 to select cells with very vigorous responses, we find that 41% ADN cells are classified as azimuth-  
204 tuned, 28% as tilt-tuned, and 28% as conjunctive. Thus, even when a stringent criterion is used,  
205 over a fourth of ADN cells exhibit large 3D responses. A sizeable, but lower, fraction of CIN cells  
206 (12% azimuth-tuned, 7% tilt-tuned, 5% conjunctive) exhibit similar strong responses. In contrast,  
207 only a minority (<3%) of RSC cells pass this threshold, indicating that significant HD responses  
208 exist in RSC but are generally weaker than in ADN, which is a known property already (Chen et al.  
209 1994). Importantly, the proportion of tilt-tuned cells is typically higher than Az-tuned cells in all  
210 areas, regardless of NTA threshold (green vs. blue curves).

211



212

213 **Supplementary Figure 8: Azimuth and tilt responses when moving freely and restrained.**

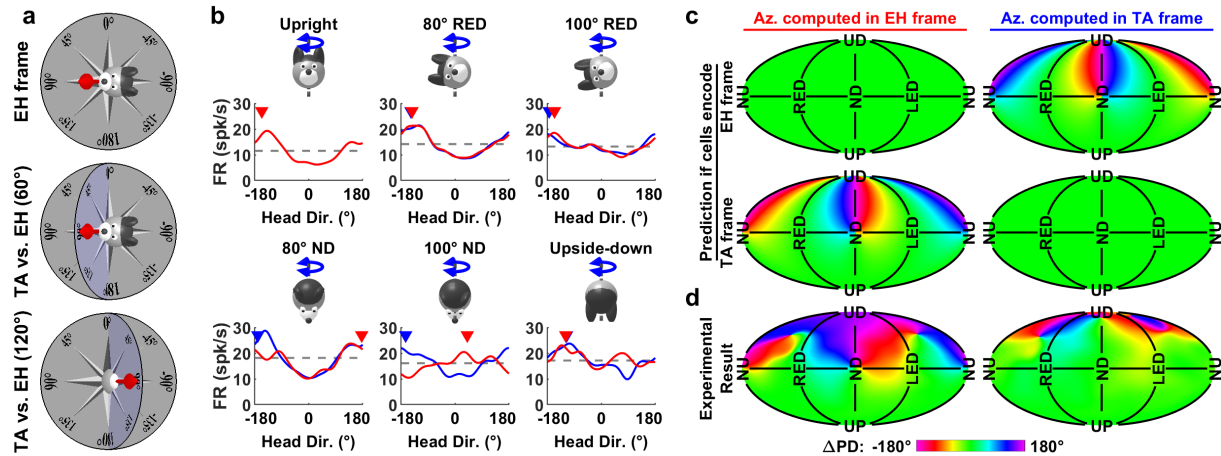
214 **(a,b)** Comparison of azimuth response amplitude when moving freely in the arena  
 215 (Experiment 1-L0,1,2; **Supplementary Table 2**) and when restrained in the rotator (Experiment  
 216 3-L, considering data for tilt < 45°). Data from cells significantly modulated to azimuth in  
 217 Experiment 1 and recorded during Experiment 3-L (n=303). Responses were attenuated in two  
 218 ways when mice were restrained: the peak firing of the cells was reduced (a; median amplitude  
 219 ratio= 1:2 [1:7.3 - 1:2.2] CI; grey) and the NTA (peak to trough amplitude divided by peak firing)  
 220 was also reduced (b: median amplitude ratio= 1:2.6 [1:2.4 - 1:2.8] CI; grey).

221 **(c-d)** Comparison of tilt response amplitude when moving freely on the platform  
 222 (Experiment 2; **Supplementary Table 2**) and when restrained in the rotator (Experiment 3-L; re-  
 223 analyzed based on data when head tilt < 60° to match the range of tilt sampled in Experiment 2).

224 Data from cells significantly modulated to tilt when moving freely and recorded during  
225 Experiment 3-L (n = 70). Both the peak responses and the NTA were attenuated (peak: median  
226 amplitude ratio= 1:1.3 [1:1.2 1:1.5] CI; NTA: median amplitude ratio= 1:1.6 [1:1.5 1:2] CI).  
227 Together, panels (a-d) indicate that restraining mice leads to an attenuation of both azimuth and  
228 tilt responses, both in terms of peak firing and in terms of response modulation relative to firing  
229 (i.e. NTA). Azimuth tuning is attenuated to a larger extent than tilt tuning (Wilcoxon rank sum  
230 tests, peak response:  $p=0.002$ ; NRA:  $p<10^{-8}$ ), which is the reason tilt tuning curves can be reliably  
231 measured in the rotator in most neurons, but azimuth tuning curves only in a minority of neurons  
232 (**Fig. 2c**).

233 **(e,f)** Inconsistency in azimuth PDs, but consistency of difference in azimuth PD between  
234 pairs of cells across setups. The arena and the rotator are different setups located in separate  
235 rooms and don't share a common azimuth reference. Therefore, the azimuth compass may  
236 anchor to a priori random orientations in each setup, which would cause the PD of individual cells  
237 to vary randomly. Accordingly, PDs shift by more than  $90^\circ$  in 29/63 cells (panel c,  $p=0.6$ , Binomial  
238 test). However, if azimuth-tuned cells are part of a neural compass, then the PD of simultaneously  
239 recorded cells should remain anchored one relative to the other. Therefore, the difference in PD  
240 between pair of cells should be identical in the arena and in the rotator. Indeed, PD differences  
241 in the arena vs. rotator were significantly conserved in panel d (within  $90^\circ$  in 44/54 pairs of cells,  
242  $p<10^{-5}$ , Binomial test). Note, however, that unlike the azimuth compass that anchors to visual  
243 landmarks, a tilt compass anchored to gravity (**Fig. 1a**), should have identical PDs on the platform  
244 and in the rotator. This is indeed the case, as shown in the pixel-by-pixel correlation of the fitted  
245 tilt tuning curves up to  $60^\circ$  tilt that could be tested in both setups (**Fig. 2d**; We used the  
246 correlation analysis for tilt tuning, because the PD of most cells can't be measured on the  
247 platform, which is restricted to  $60^\circ$  tilt. Also note that together, panels a-d and **Fig. 2** indicate that  
248 the spatial tuning characteristics of both azimuth and tilt tuning are conserved across free  
249 locomotion and restrained, passive motion, and that, other than the smaller response  
250 magnitude, the 3D responses measured in the rotator are representative of the neurons' natural  
251 responses.





252

253 **Supplementary Figure 9: Azimuth tuning is spatially invariant when expressed in a TA frame.**

254 (a) Illustration of the EH and TA model (equivalent to the dual-axis rule<sup>7,8</sup>). In an EH frame  
 255 (top panel), head direction is projected onto the EH plane (grey). In a TA frame, head direction is  
 256 measured in a compass (blue) that is coplanar with the head horizontal plane and oriented such  
 257 that the azimuth measured in the EH and TA frame coincide along the line of intersection of both  
 258 planes (the 0-180° axis here). In other words, the TA frame is anchored to the allocentric  
 259 reference frame along the earth-horizontal direction. It is defined by rotating a horizontal  
 260 compass to align with head direction, instead of projecting head direction onto the horizontal  
 261 plane (EH frame). In the example orientations shown here, the head pitches upward by 60°  
 262 (middle panel) and 120° (bottom panel). In a TA frame, it faces 90° in both panels. When  
 263 projected onto the EH plane, its direction reverses from 90° to -90° when pitch angle exceeds  
 264 90°, as reported by Finkelstein et al.<sup>9</sup>. Note that, if the head is facing the 0° (or 180°) direction, it  
 265 would be rolling instead of pitching, and azimuth reversal would not occur since these directions  
 266 coincide in the EH and TA frames. As a general rule, TA is reversed relative to EH azimuth when  
 267 tilt angle exceeds 90° in the pitch plane, but not in the roll plane. In intermediate tilt planes, the  
 268 difference between EH and TA azimuth depends of tilt angle (see panel c).

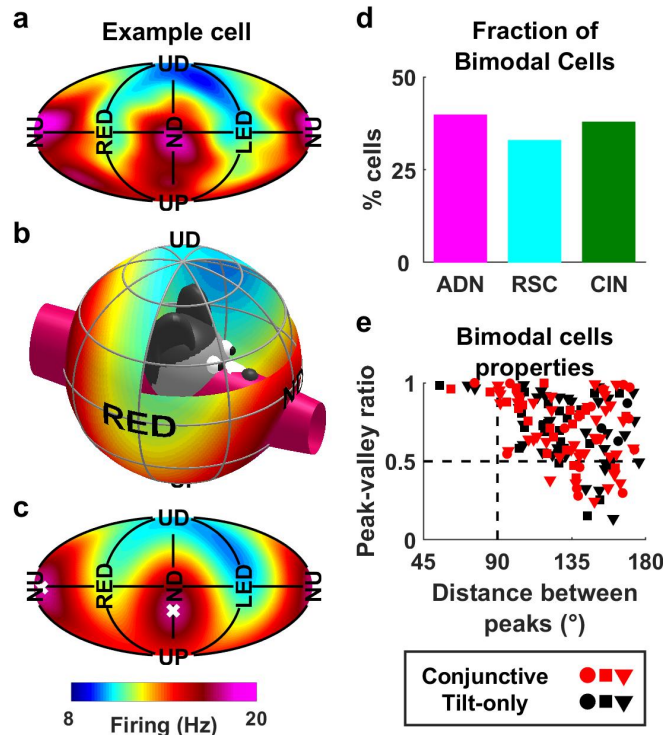
269 (b) Azimuth tuning curves of an example cell, extracted from the full 3D tuning curve  
 270 measured in Experiment 3-L and computed in EH (red) or TA (blue) reference frames. Each curve  
 271 represents the firing rate for all possible azimuths at a single tilt angle, which correspond to the  
 272 positions attained by tilting the head to a given Dir. orientation and rotating around an earth-vertical  
 273 axis (see **Supplementary Movie 1**). Note that the azimuth response of the example cell is modest

274 since azimuth tuning is reduced when measured in a rotator (see **Supplementary Fig. 8a,b**). In an  
275 EH frame, the cell's PD (-157°) was conserved for tilt orientations in the roll plane (-143° and -  
276 156° at 80° and 100° RED) but reversed abruptly for tilt angles larger than 90° in the pitch plane  
277 (from 177° to 41° at 80° and 100° ND). However, there is no such abrupt reversal when azimuth  
278 is computed in the TA frame.

279 **(c)** Predicted change of the cell's azimuth PD in tilted orientations ( $\Delta$ PD, expressed relative  
280 to its PD when upright), displayed as a color map. For a given 3D head orientation, azimuth differs  
281 when computed in a EH or TA frame. The difference between both azimuths depends on the  
282 head's orientation relative to gravity (see **Online Methods**). If cells encode azimuth in an EH  
283 frame, we expect their PD to be invariant across all head tilts (i.e.  $\Delta$ PD $\approx$ 0) when azimuth is  
284 expressed in the EH frame (upper left panel) but to vary with head tilt, and in particular to reverse  
285 when the head is pitched beyond 90° (i.e. between NU/ND and UD) when azimuth is expressed  
286 in TA frame (upper right panel). Reciprocally, if cells encode azimuth in a TA frame, we expect  
287 their PD to be invariant when expressed in a TA frame (lower right panel) but to vary when  
288 expressed in EH frame (lower left).

289 **(d)** Average  $\Delta$ PD across all azimuth-tuned cells significantly tuned to azimuth in  
290 Experiment 3-L (17 ADN, 7 RSC, 39 CIN). The azimuth PD varies when expressed in an EH frame  
291 but remains invariant (except close to UD) when expressed in a TA frame, in line with predictions  
292 of the TA model. Note that the PD becomes more variable close to UD, likely because azimuth  
293 tuning amplitude is near zero close to UD (see **Fig. 3g**), making data unreliable at this orientation.

294



295

296 **Supplementary Figure 10: The model of 3D gravity tuning explains bimodal tilt tuning curves.**

297 **(a)** Example cell exhibiting two response peaks, in ND and NU orientation.

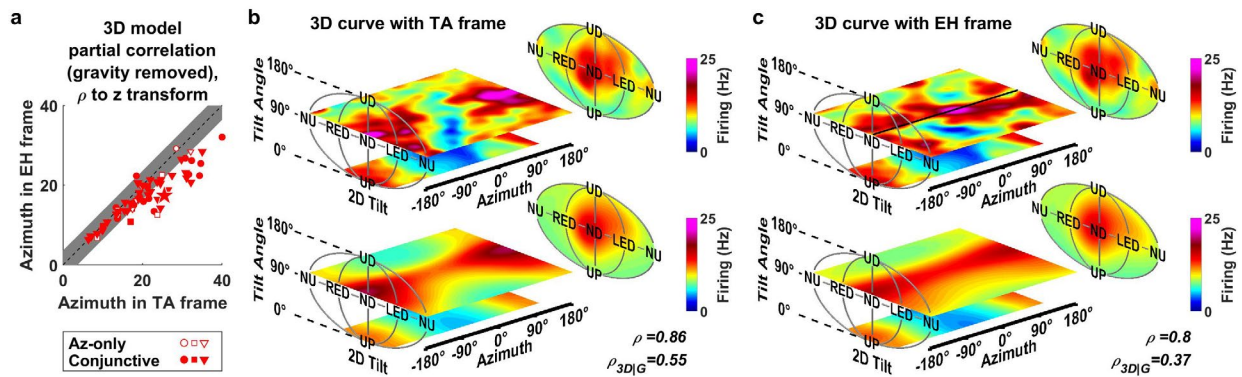
298 **(b)** 3D Gaussian tuning model. Gravity tuning is modeled as a 3D Gaussian tuning curve in  
 299 egocentric Cartesian space (ellipsoid in **Fig. 4a**). In this cell, the 3D Gaussian, shown as a purple  
 300 ellipsoid (indicating points located within 0.4 standard deviation from the Gaussian's center; the  
 301 ellipse's color corresponds to the cell's firing rate at these points) is markedly elongated (the  
 302 extremities of the ellipsoid are truncated to fit in the figure). Gravity on earth has a constant  
 303 magnitude and is restricted to a 2D sphere around the head. The ellipsoid intersects this sphere  
 304 at two positions (close to ND and NU orientation, i.e. when the gravity vector is aligned with the  
 305 X axis).

306 **(c)** Same tuning curve as in (b), where the sphere has been projected onto the figure's  
 307 plane. The two peaks are marked by white dots. The tuning curve matches the raw tuning curve  
 308 in (a) (correlation coefficient  $\rho=0.98$ ). Thus, from a practical point of view, the cell appears  
 309 bimodal as it responds preferentially at two distinct head tilts; but from a mechanistic point of  
 310 view its tuning can be explained by processing sensory signals through a unimodal Gaussian  
 311 distribution.

312           **(d)** We identified bimodal tuning by fitting all cells with the 3D Gaussian model and  
313 counting the number of local maxima on the 2D tilt tuning curve (i.e. on the sphere). All cells have  
314 either one (unimodal) or two (bimodal) local maxima. The proportion of bimodal cells in each  
315 region is shown. Overall, 36% (141/388) tilt-tuned cells were bimodal. This proportion is similar  
316 in each region (Chi square test,  $p=0.56$ ,  $\chi^2=1.15$ , 2 dof), across conjunctive and tilt-only cells (Chi  
317 square test,  $p=0.68$ ,  $\chi^2=0.17$ , 1 dof), and across cells tuned in the pitch or roll plane (Chi square  
318 test,  $p=0.29$ ,  $\chi^2=1.14$ , 1 dof).

319           **(e)** We further characterized bimodal tuning curves by computing the angular distance  
320 between the two peaks (abscissa) and the ratio of the peak-valley amplitude of the two peaks  
321 (smallest/largest peak; ordinate). In the example cell in (c), the distance is  $151^\circ$ , i.e. the two peaks  
322 are almost opposed, and the amplitude ratio is 0.97, i.e. the two peaks have nearly equal  
323 magnitude. We find that the two peaks are well separated (distance  $> 90^\circ$ , 135/144 cells, 96%)  
324 and have comparable magnitudes (ratio  $> 0.5$ , 116/144 cells, 83%) in most bimodal cells.

325



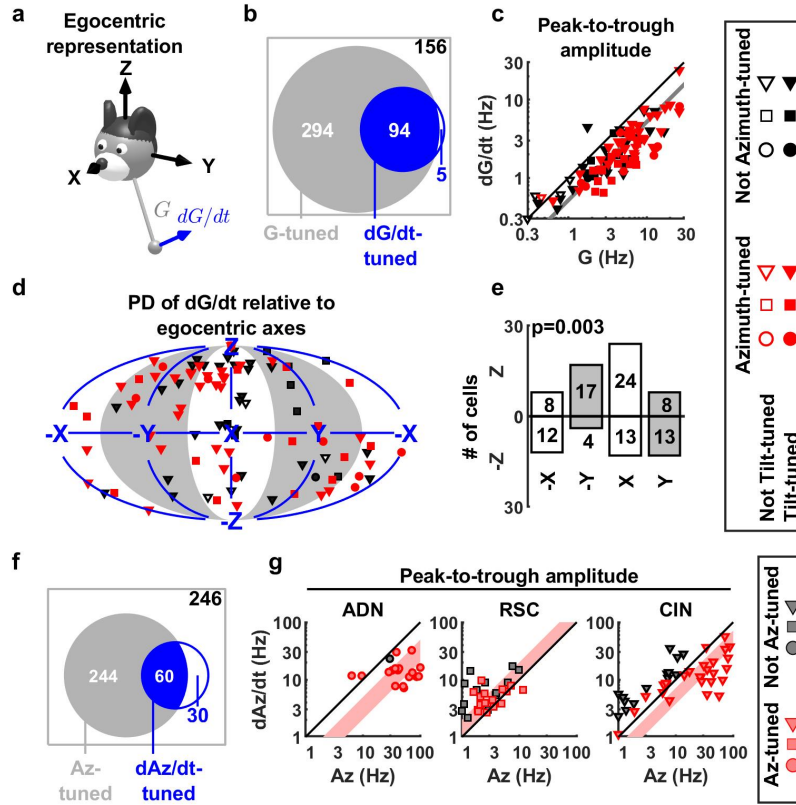
326

327 **Supplementary Figure 11: Comparison of 3D model fitting with azimuth in TA or EH frame.**

328 **(a)** Partial correlation of the model fits (shown as z-score), with the correlation  
 329 attributable to gravity removed so that the partial correlation reflects how the model fits azimuth  
 330 tuning in 3D. Data for all Az-tuned neurons that maintained their azimuth tuning in the rotator  
 331 (Experiment 3-L) when the head is close to upright (<45° tilt; 17 ADN, 7 RSC, 39 CIN). Grey band:  
 332 zone where partial correlations are not significantly different at  $p < 0.01$ . Partial correlations were  
 333 significantly higher when azimuth was expressed in a TA frame in 24/63 neurons, and significantly  
 334 higher in a EH frame in only 1 ADN neuron (in this neuron, the difference between both frames  
 335 was weak and vanished if only data for > 90° tilt was analyzed, indicating that it is likely a false  
 336 positive). This analysis confirms that neuronal responses are more consistently expressed in a TA  
 337 frame. The absence of significant difference in a large fraction of neurons (38/63) is explained by  
 338 both the similarity between TA and EH frames at small tilt angles and the tendency of azimuth  
 339 responses to decrease with tilt angle (see **Fig. 3f,g**). An alternative explanation, which would be  
 340 that cells encode a mixture of EH and TA azimuth, may be rejected because the two frames are  
 341 mutually exclusive.

342 **(b,c)** 3D tuning curve of an example neuron computed in both frames (upper panels) and  
 343 corresponding model fits (lower panels). This neuron was tuned to tilt, with a PD at  $\alpha = 100^\circ$  tilt in  
 344 ND orientation ( $\gamma = -5^\circ$ ), as well as azimuth with a PD at  $-175^\circ$  when upright (lower planes in the  
 345 3D curve). TA and EH frames are identical near upright and, accordingly, tuning appears similar.  
 346 Next, we examine tuning at a tilt angle of  $100^\circ$  (upper planes), where the TA and EH frames  
 347 diverge sharply (as in **Supplementary Fig. 9a,c**). In a TA frame (b), the cell still exhibited a clear  
 348 azimuth tuning with a similar PD ( $168^\circ$ ) as in upright. The 3D model (lower panel) captured the  
 349 3D curve by multiplying a tilt tuning centered on  $100^\circ$  ND with an azimuth tuning curve centered

350 on 175°, leading to a total correlation of  $\rho=0.86$  and a partial correlation of  $\rho_{3D|G}=0.55$ . In contrast,  
351 azimuth tuning was largely distorted when expressed in a EH frame (upper plane on panel c). In  
352 ND orientation (marked by a black line), the cell's response reversed and peaked at an azimuth  
353 of 18° (magenta). In contrast, it shifted back to  $\pm 180^\circ$  on either side of the line, i.e. when head  
354 orientation neared RED and LED. This pattern, where azimuth tuning reverses in ND but not RED  
355 or LED, corresponds to the reversal of TA azimuth relative to EH azimuth (**Suppl Fig. 15a,c**) and is  
356 expected if azimuth is encoded in a TA frame. Therefore, the cell's azimuth PD was not invariant  
357 relative to head tilt when expressed in an EH frame. Since this violates the assumption of the 3D  
358 model, the correlation decreased to  $\rho=0.8$  and  $\rho_{3D|G}=0.37$  (note that the correlation didn't  
359 decrease to zero since the model could still fit azimuth tuning at low tilt angles).  
360



361

362 **Supplementary Figure 12: Responses to tilt and azimuth velocity.** We used identical criteria to  
 363 assess whether cells were significantly tuned to azimuth velocity ( $dAz/dt$ ) and tilt velocity (i.e.  
 364 the time derivative of gravity,  $dG/dt$ ) (see Methods).

365 (a) Gravity derivative was expressed in an egocentric (X,Y,Z) frame, similar to gravity, and  
 366 the responses to gravity derivative was fitted with Gaussian functions (as in **Supplementary Fig.**  
 367 **10**).

368 (b) A small percentage of cells (99/549, 18%) exhibited significant tuning to tilt velocity  
 369 (data from Experiment 3-L; **Supplementary Table 2**). Furthermore, the majority (94/99; 95%) of  
 370 these were also tuned to tilt. Tilt-tuned cells were more likely to be tuned to  $dG/dt$  (Chi square  
 371 test,  $p < 10^{-8}$ ,  $\chi^2 = 34$ , 1 dof).

372 (c) For most cells, tilt velocity responses had a lower amplitude than tilt position  
 373 responses (geometrical average ratio = 0.48, [0.44 0.54] CI; data from  $n = 94$  cells with significant  
 374 tilt and tilt velocity tuning). There were only slight differences between areas (ratio = 0.47; 0.4  
 375 and 0.55 in ADN, RSC and CIN respectively; Kruskal-Wallis ANOVA,  $p = 0.02$ ).

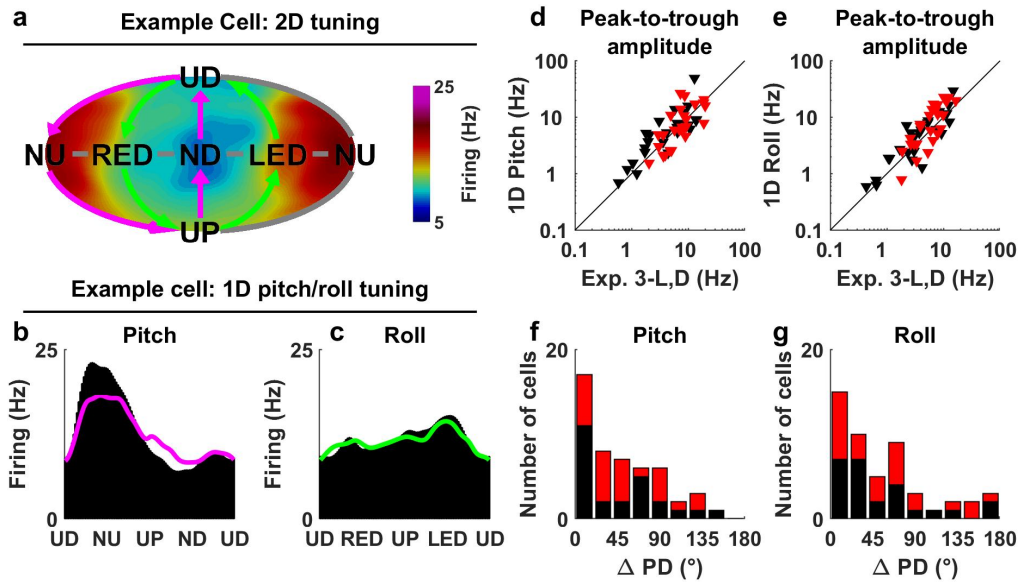


376           **(d)** Distribution of PDs for tilt velocity. **X, Y, Z** indicate that cells fire preferentially when  
377  $dG_x/dt > 0$ ,  $dG_y/dt > 0$ , and  $dG_z/dt > 0$ , respectively. **-X, -Y, -Z** indicate that cells fire preferentially  
378 when  $dG_x/dt < 0$ ,  $dG_y/dt < 0$ , and  $dG_z/dt < 0$ , respectively.

379           **(e)** Number of cells in all 8 quadrants of panel d. Most cells prefer  $dG_z/dt > 0$ , and  $dG_x/dt > 0$ ,  
380 i.e. when the gravity vector moves forward and upward in head coordinates, which corresponds  
381 from instance to ND pitch movements when starting from an upright condition. P-value based on  
382 a  $\chi^2$  test versus uniform distribution.

383           **(f)** A small percentage of cells (90/580, 16%) was also tuned to azimuth velocity ( $dAz/dt$ ).  
384 19% of azimuth-tuned cells were tuned to  $dAz$ , versus 11% of non azimuth-tuned cells (Chi square  
385 test,  $p=0.003$ ,  $\chi^2=8.6$ , 1 dof).

386           **(g)** For cells tuned to both  $Az$  and  $dAz/dt$ ,  $Az$  velocity responses had a lower amplitude  
387 than  $Az$  position (direction) responses in ADN (median ratio: 1:3.1, [2-4.9] CI;  $p < 10^{-3}$ , signed rank  
388 test), but in contrast were slightly larger in RSC (median ratio 1.5:1, [1.1-2] CI;  $p < 10^{-3}$ ). The ratio  
389 in CIN was intermediate (2:1 in favor of  $Az$  responses, [1.4-2.8] CI;  $p < 10^{-5}$ ). The peak-to-trough  
390 amplitude of  $dAz/dt$  tuning curves, measured across the range of  $\pm 200^\circ/s$ , had a median value of  
391 13 Hz ([11-15] CI) in ADN, 5.5 Hz; [3.7-6.6] CI) in RSC. The distribution of responses in CIN  
392 resembled a mixture of ADN cells (with high  $Az$  and lower  $dAz$  responses) and RSC cells (with low  
393  $Az$  and  $dAz/dt$  responses).



394

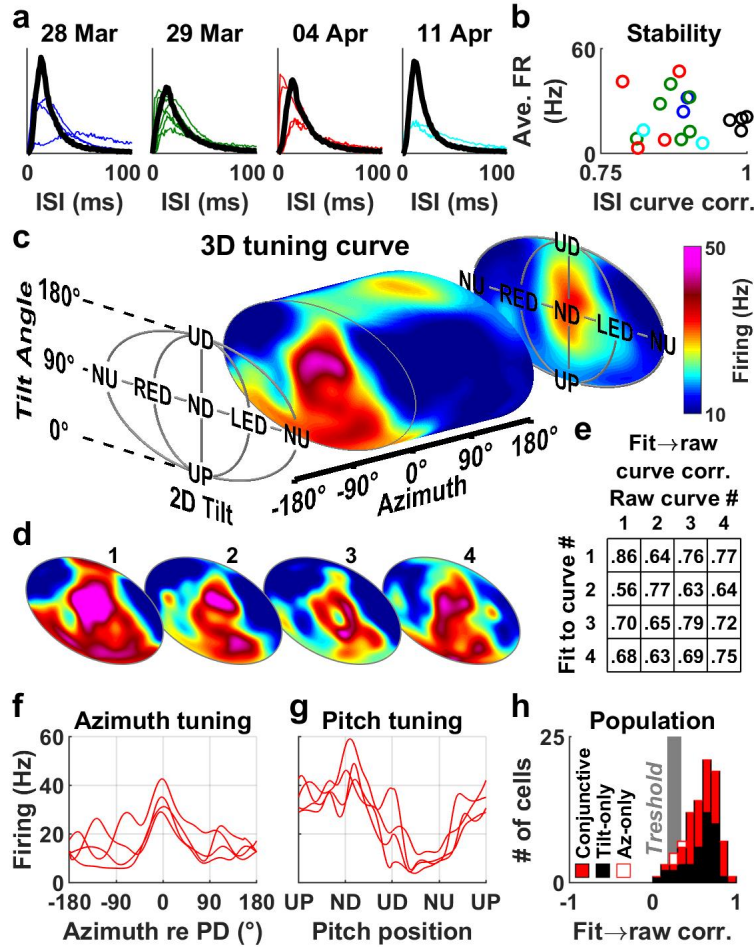
395 **Supplementary Figure 13: Comparison between pitch/roll rotation and 3D rotation.**

396 **(a)** Average tilt tuning curve of an example cell (same as in Fig. 1I). During pitch rotation,  
 397 the head is tilted from upright to ND, UD, NU and back to upright, as illustrated by magenta  
 398 arrows. During roll rotation, the head is tilted from upright to LED, UD, RED and back to upright  
 399 (green). Rotations in the opposite sequence are also performed.

400 **(b, c)** average firing rate during pitch and roll (magenta and green curves). The firing rate  
 401 measured at corresponding tilt positions during Experiment 3-L,D (3D rotations) is shown in  
 402 black. Both curves match well, indicating that responses during complex 3D trajectories  
 403 generalize to simple 1D rotation.

404 **(d, e)** Peak-to-trough modulation amplitude measured during pitch/roll (ordinate) vs. that  
 405 predicted based on tilt tuning curves measured in Experiment 3-L,D (abscissa). Amplitudes are  
 406 significantly correlated ( $p < 10^{-10}$  for both pitch and roll;  $n = 50$  tilt-tuned cells, data averaged across  
 407 recordings in light and darkness). The responses are slightly higher during single axis rotation in  
 408 roll (median = 5.9 vs 3.8 Hz;  $p = 10^{-3}$ , signed rank test) but not pitch (median = 6.4 vs 4.4 Hz;  $p = 0.3$ ,  
 409 signed rank test).

410 **(f, g)** Distributions of absolute difference in tilt preferred direction (PD) between 1D and  
 411 3D stimuli for pitch and roll planes, respectively. Both are significantly aligned with 0  
 412 (Kolmogorov-Smirnov tests to test the difference with a uniform;  $p < 10^{-5}$  in both). Red  
 413 symbols/bars: Azimuth-tuned cells; Black symbols/bars: Not-azimuth-tuned cells.



414

415 **Supplementary Figure 14: Reproducibility of 3D tuning across days.**

416 **(a)** ISI distribution of a neuron recorded 4 times during Experiment 3-L, on 4 distinct days  
 417 spanning a 2-week period (black). The tetrode was not moved in this period. The ISI distribution  
 418 of all other neurons recorded on the same tetrodes are shown in color.

419 **(b)** Identification of the neuron across the 4 recordings. We display the average firing of  
 420 all neurons in (a), colored using the same code as in (a), versus the correlation between all ISI  
 421 curves and the black ISI curve on March 28. The black dots form a cluster on the right side of the  
 422 graph, indicating that the shape of the ISI curve and the cell's firing rate are distinct enough to  
 423 identify across days. Note that we used only spike waveforms, mean firing and ISI distribution to  
 424 identify neurons across multiple experiments within a single day. In contrast, we also considered  
 425 tuning curves when identifying neurons across separate days, and only considered spiking activity  
 426 recorded in separate days to originate from the same neurons if 3D tuning curves were similar.  
 427 Thus, we were able to identify neurons that exhibit stable tuning over several days. In contrast,

428 we can't determine whether some neurons have unstable tuning over days since, even if we  
429 recorded such neurons during multiple days, we wouldn't be able to determine that the  
430 recordings originate from the same neuron. Thus, this figure demonstrates that some neurons  
431 can maintain a stable 3D tuning across days but doesn't imply that the 3D tuning of some HD cells  
432 can't drift over days. Over 549 cells, we recorded Experiment 3-L on 2 distinct days in 63 cells, 3  
433 days in 15 cells, and 4 days or more in 13 cells.

434 **(c)** 3D tuning curve of the example cell (conjunctive cell in CIN; same as in **Supplementary**  
435 **Movie 8**). A vertical section of the 3D tuning curve is shown at an azimuth of  $0^\circ$  that corresponds  
436 to the cell's PD. Data averaged across all repetitions of Experiment 3-L.

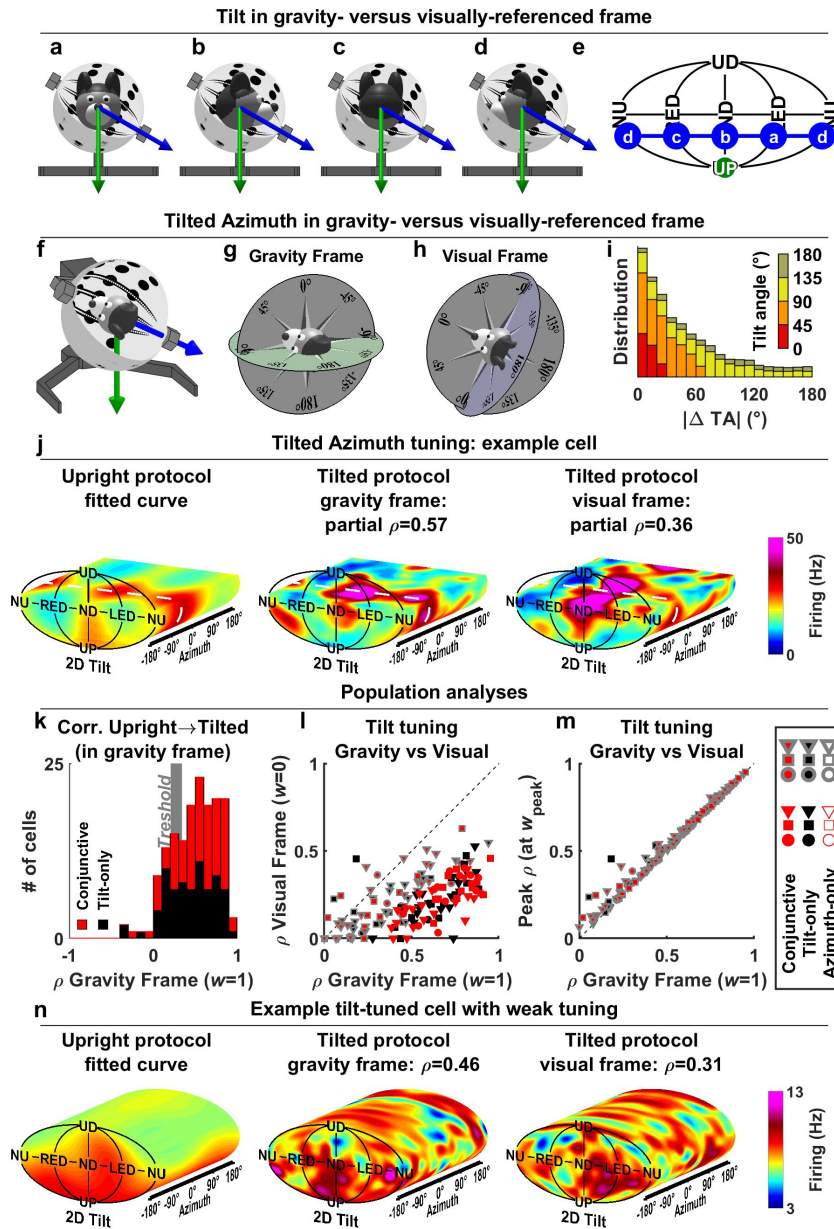
437 **(d)** Reproducibility of the tuning curve. The cell's response was recorded 4 times during  
438 Experiment 3-L, on 4 distinct days spanning a 2-week period. 3D tuning curves were recomputed  
439 for each repetition. The same vertical section as in (a) is shown for all repetitions (labelled 1 to  
440 4), using the same color scale. Peak firing occurs consistently in the vicinity of ND orientation.

441 **(e)** We evaluated tuning stability by fitting the 3D model to the 4 tuning curves, and  
442 computing the pixel-by-pixel correlation between the model fits and the raw curves. The  
443 correlations are shown on a matrix; the average correlation over off-diagonal elements, i.e.  
444 across different repetitions, is 0.67.

445 **(f)** Azimuth tuning curve in upright orientation extracted from the 4 3D tuning curves, and  
446 centered on each curve's PD.

447 **(g)** Pitch tuning curve extracted from the 3D tuning curves, at the azimuth corresponding  
448 to each curve's PD. Analyses in panels d to g indicate that 3D responses (or responses along 1D  
449 yaw and pitch trajectories) were stable across several days in the example cell.

450 **(h)** Distribution of the average correlation between repetitions of Experiment 3-L (as in  
451 panel e), for all tuned cells ( $n=90$  cells; 47 conjunctive, 40 tilt only, 3 azimuth-only). We used a  
452 shuffling procedure to determine the threshold value over which the correlation is significant (at  
453  $p<0.01$ ) on a cell by cell basis. The average threshold across cells is  $0.26 (\pm 0.04 \text{ s.d.})$ , interval shown  
454 in grey). 94% of cells pass the significance threshold, with the median correlation being 0.63  
455 ( $[0.57-0.67]$  CI), similar for conjunctive and tilt-only cells (Wilcoxon rank sum test,  $p=0.46$ ) and  
456 cells with PD in the pitch and roll planes ( $p=0.49$ ).



457

458 **Supplementary Figure 15: Protocol 3-T.**

459 **(a-e)** Comparison of tilt tuning computed relative to gravity-referenced (green) or  
 460 visually-referenced (blue) vertical. Panels a-d illustrate position situations where the head is  
 461 upright relative to gravity (UP point in panel e) but tilted 60° (along 4 different directions)  
 462 relative to the visually-referenced vertical axis (marked a-d in panel e). As a rule, during the 3D  
 463 rotation protocol, the gravity-referenced and visually-referenced verticals always differ by exactly 60°.

464 **(f-i)** Comparison of TA azimuth measured in a gravity- or visually-referenced frame. Panel  
 465 f: example 3D head orientation. Panels g-h: representation of the earth-horizontal compass in a

466 gravity-referenced (f, green) and visually-referenced (h, blue) frame. Tilted azimuth is measured  
467 by rotating the earth-horizontal compass in alignment with the head-horizontal plane, resulting  
468 in the grey compasses in panels g-h. In this example, the resulting azimuth is 60° and 2° in panels  
469 g and h respectively, i.e. a difference of 58°. Panel i: the difference between TA in a gravity-  
470 referenced or visually-referenced frame is a complex function of 3D head orientation. To  
471 appreciate how they differ in practice, we computed the difference in TA between these frames  
472 ( $|\Delta TA|$ ) over the whole protocol, color-coded as a function of tilt angle (in either frame).  
473 Although the  $|\Delta TA|$  is minimal for small head tilts (e.g. <45°, red: median  $|\Delta TA| = 10^\circ$ ), it  
474 increases for larger tilt angles (e.g. larger than 45° and lower 135°; orange-yellow; median  $|\Delta$   
475  $TA|=37^\circ$ ). Since HD cells still exhibit appreciable azimuth responses in this range of tilt, it is  
476 possible to use this protocol to determine the frame in which they encode TA.

477 **(j)** Example conjunctive cell. Left: reference tuning function fitted to the response  
478 measured with the rotator upright. A section of the tuning curve at 105° tilt is shown. The cell  
479 fires preferentially at an azimuth of -77° (broken white line). Middle and right: experimental  
480 tuning curves measured with the rotator tilted and computed with tilt expressed in a gravity-  
481 referenced frame, and azimuth expressed in a gravity-referenced (middle) or visually-referenced  
482 (right) frame. Azimuth tuning is well preserved when expressed in a gravity-reference frame  
483 (middle) but not in a visually-referenced frame (left). Accordingly, the partial correlation between  
484 the reference tuning curve (left) and the experimental tuning curves (middle, right) is higher  
485 when azimuth is expressed in a gravity-reference frame ( $\rho=0.32$  versus 0.13; partial correlation  
486 computed by removing the effect of gravity tuning, see Methods).

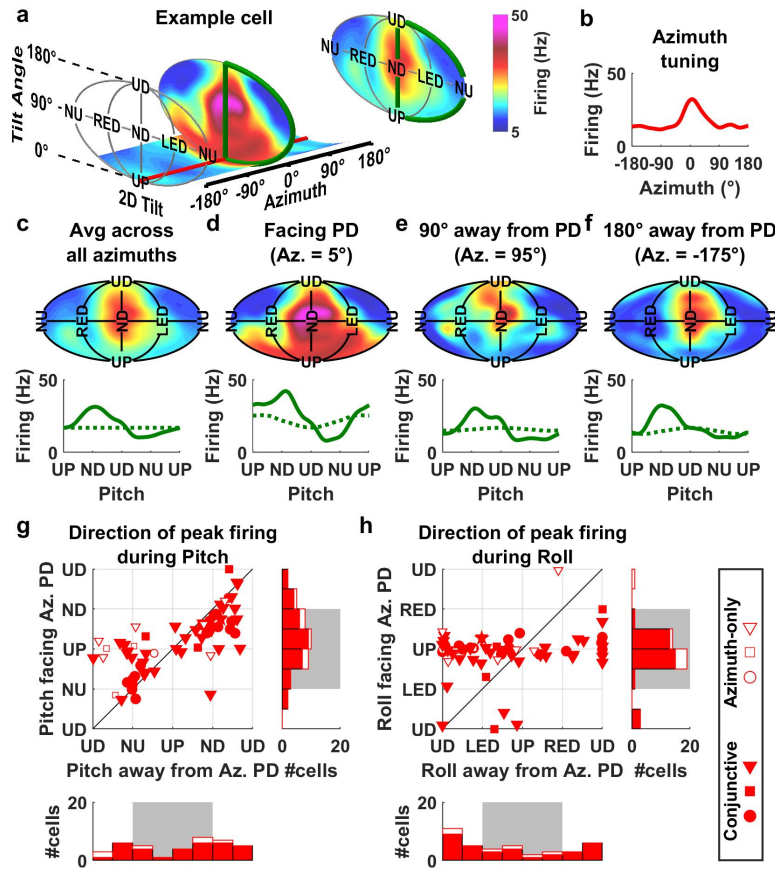
487 **(k)** Stability of 3D tuning when recorded with the rotator upright and tilted. We plot the  
488 distribution of  $\rho$  computed in a gravity-referenced frame (see **Fig. 6a,b**). We used a permutation  
489 test to determine if  $\rho$  was significantly higher than 0 on a cell-by-cell basis (mean threshold value:  
490 0.11; SD=0.03; vertical grey band).  $\rho$  was significantly higher than 0 in 135/148 tilt-tuned cells  
491 (19/22 ADN; 38/46 RSC; 68/80 CIN; permutation test,  $p<0.01$ ). Cells in which  $\rho$  was not  
492 significantly higher than 0 typically have lower peak firing rate (5.7 vs 13.2 Hz,  $p=0.007$ , Wilcoxon  
493 rank sum test). The median value of  $\rho$  was 0.53 ([0.45-0.57] CI).

494           **(l,m)** Additional analyses of tilt tuning (see **Fig. 6**). Panel l: Even though, at the population  
495 level,  $w_{peak}$  accurately centered on 1 (**Fig. 6d**), we observed that it was close to zero (or at least  
496 lower than 0.5) in a few cells (3%). To investigate whether a subpopulation of cells may encode  
497 visually-referenced tilt, we tested if the correlation  $\rho$  is significantly higher when tilt is expressed  
498 in a gravity or visual frame on a cell-by-cell basis. As expected,  $\rho$  was significantly higher in a  
499 gravity reference frame in 78/148 cells (15/22 ADN; 26/46 RSC; 37/80 CIN). The difference  
500 between the two frames was non-significant in all other cells (markers with grey border) but one  
501 black (marker about the diagonal), which is weakly modulated cell and likely a false positive.  
502 Panel m: we test if some cells may use an intermediate reference frame by comparing the  
503 correlation when tilt is expressed in a gravity reference frame ( $w=1$ ) or at the peak of the  
504 distribution ( $w_{peak}$ ). Data points lie close to the diagonal since the peak is generally close to 1.  
505 Importantly, the peak correlation is significantly higher than the correlation in a gravity frame in  
506 only one cell (likely false positive, same as in panel k), indicating that cells don't use intermediate  
507 reference frames.

508           **(n)** Example tilt-tuned cell where the correlation  $\rho$  was similar in a gravity-referenced  
509 (middle panel) and visually- referenced (right) frame. This cell had a low modulation amplitude  
510 (tilt modulation amplitude = 2.9 Hz; NTA=0.32). As a result, the tuning curves recorded with the  
511 rotator tilted were markedly flat and noisy in both reference frames; and the correlations  
512 weren't significantly different. Similarly, cells where the correlations in gravity- and visually  
513 referenced frames (symbols with grey outlines in panel l) had lower tilt modulation amplitude  
514 (median peak-valley modulation: 4.2 versus 6.35 Hz,  $p=0.002$ , Wilcoxon rank sum test; median  
515 NTA = 0.39 versus 0.52,  $p=0.002$ ) and, being comparatively noisier, were generally poorly  
516 correlated (median  $\rho$ : 0.3 versus 0.67 in gravity frame, 0.18 versus 0.24 in visual frame).

517





518

519 **Supplementary Figure 16: Possible bias when measuring pitch/roll tuning in azimuth-tuned**

520 **cells** (see also Laurens and Angelaki, 2019, ref<sup>10</sup>). A recent study in rat ADN (Shinder and Taube,

521 2019, ref<sup>11</sup>) failed to identify tilt responses in a sample of 24 azimuth-tuned HD cells. In that study,

522 mice were positioned upright, facing the azimuth PD, and rotated in pitch and/or roll. The authors

523 observed that most cells fired more in tilt positions near upright and concluded on that account

524 that there is “limited evidence that cells contained conjunctive firing with pitch or roll position”

525 (sic). Here we demonstrate that the experimental protocol used by Shinder and Taube<sup>11</sup>, where

526 mice were tilted while facing the cell’s PD, tends to conceal pitch/roll tuning, because it is

527 superimposed on a strong azimuth tuning, whose strength is reduced as a function of head tilt

528 (**Fig. 3f,g**). We show that, had we used the same experimental protocol and analyses, we would

529 have failed to see robust tilt tuning as well.

530 **(a)** 3D tuning curve of an example conjunctive cell (measured during Experiment 3-L;

531 same cell as in **Fig. 4c** and **Supplementary Fig. 14**). When averaged across all azimuths (rightmost

532 plane), the cell is tuned to tilt with a PD in ND. The cell is also tuned to azimuth, with a PD at 5°.

533 A vertical section (i.e. firing rate for all tilt positions at a given azimuth) of the tuning curve is  
534 shown at the azimuth PD. When exclusively tested during pitch in this plane (green line; as  
535 Shinder and Taube, 2019<sup>11</sup>, did), the cell's tilt modulation is much broader and the cell's firing at  
536 ND is barely above its firing when the animal is upright (red).

537 **(b)** Average azimuth tuning curve when upright, peaking at 5°.

538 **(c)** Analysis in this study: Upper panel: Tilt tuning curves averaged across all azimuth  
539 angles (as in panel a). Lower panel: Firing rate measured along a pitch trajectory; Solid green  
540 curves: actual data; Dashed green curves: simulated data (see below).

541 **(d)** Experiment by Shinder and Taube, 2019<sup>11</sup>: Tilt tuning was tested when animals faced  
542 the azimuth PD. Note that firing is elevated in the vicinity of upright. Even though the firing is  
543 largest in ND, the preferred pitch direction, evaluated by fitting a von Mises function, is biased  
544 towards upright (67° ND tilt in d versus 108° ND tilt in c).

545 **(e,f)** Tilt tuning tested 90° (e) or 180° (f) away from the cells' azimuth PD. Firing measured  
546 during pitch rotation away from the PD is similar as the average curve in (c). We use the 3D  
547 model fit to demonstrate that the curve in (d) is affected by azimuth tuning. We fit the cell's 3D  
548 tuning curve, then alter the model's parameter to eliminate tilt tuning (by setting  $A$  to 0 and  $FR_0$   
549 to the cell's average firing in  $FR_{Ti}(\alpha, \gamma)$ ; see **Methods**). Next we simulate the pitch tuning curve  
550 (dashed green curves) that is now influenced entirely by its azimuth tuning. The resulting curve  
551 peaks in UP orientation in (d), but is flat in other panels. This indicates that azimuth tuning affects  
552 the cell's response when facing the azimuth PD (d), such that it biases the firing rate towards  
553 upright (by interacting multiplicatively) but has little effect when facing away from the azimuth  
554 PD (e,f) or when data are averaged across all azimuths (c). We note that the green curve in (d)  
555 resembles most example pitch or roll tuning curves shown by Shinder and Taube's study<sup>11</sup>. Based  
556 on these simulations, we predict that, had the authors analyzed individual pitch/roll tuning curves  
557 recorded when the mouse faced away from the cell's PD (e, f), they would have seen tilt tuning  
558 with preferred tilt away from upright.

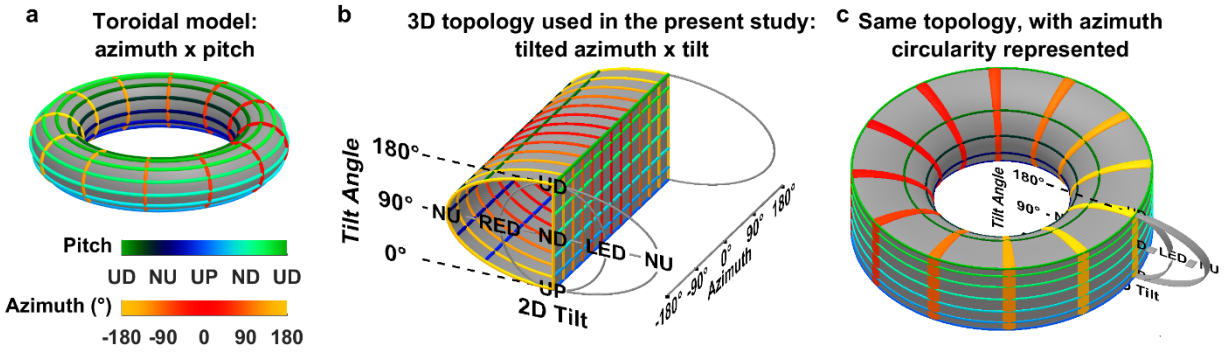
559 **(g,h)** Same analysis, at the population level. We simulated pitch/roll rotations for all  
560 azimuth-tuned cells that were also azimuth tuned in the rotator ( $n=63$ ; 53 conjunctive and 10  
561 azimuth-only cells). Top: Scatter plot showing how pitch rotations while facing the cell's azimuth

562 PD can bias conclusions. Peak responses (by fitting von Mises functions) to pitch and roll rotations  
563 when facing the azimuth PD (ordinate; as in Shinder and Taube's study<sup>11</sup>) and when facing away  
564 from the azimuth PD (abscissa). Bottom and right: Marginal distributions are shown as  
565 histograms.

566 When pitching while facing the azimuth PD (panel g), most conjunctive cells fire preferentially  
567 close to upright right-side histogram, grey zone, red bars (41/53, 78%,  $p < 10^{-4}$ ), similar to the  
568 example cell in a-f. When adding azimuth-only cells (open symbols/bars), the proportion of cells  
569 firing preferentially close to upright is maintained at 49/63 (77%). The bias is even more drastic  
570 in roll (panel h; because tilt tuning is weaker in roll), with the 49/53 conjunctive cells firing  
571 preferentially around upright (lower histogram, grey zone, red). In contrast, when pitching or  
572 rolling away from the azimuth PD (g,h; abscissae), half of the conjunctive cells (solid red  
573 symbols/bars, 24/53 in g, 19/53 in h) are not significantly different from 50%,  $p = 0.6/0.05$  respectively)  
574 fire preferentially close to upright (grey band in the marginal distribution) and the other half fire  
575 preferentially closer to UD. Thus, while recording from our neurons, if we had done the  
576 experiment (pitch/roll when animal faced azimuth PD in a small sample of cells) and analyses as  
577 in Shinder and Taube's study<sup>11</sup>, we would likely not have been able to identify tilt tuning.

578 We conclude that our dataset and quantitative analyses predict that, even though the PD of tilt  
579 tuning is distributed uniformly between upright and inverted orientation (**Fig. 5a**), conjunctive  
580 cells would appear to respond preferentially in upright orientation when recorded and analyzed  
581 as in Shinder and Taube's study<sup>11</sup>. The results published in our study are therefore entirely  
582 compatible with those described by Shinder and Taube's study<sup>11</sup>. The conclusions are opposite  
583 because the systematic scanning of 3D orientation (rather than a limited subset) allowed us to  
584 reveal tilt tuning, that was concealed by azimuth tuning in the Shinder and Taube's study<sup>11</sup>. For  
585 more details about modeling the experimental findings of Shinder and Taube<sup>11</sup>, see Laurens and  
586 Angelaki (2019)<sup>10</sup>.

587



588

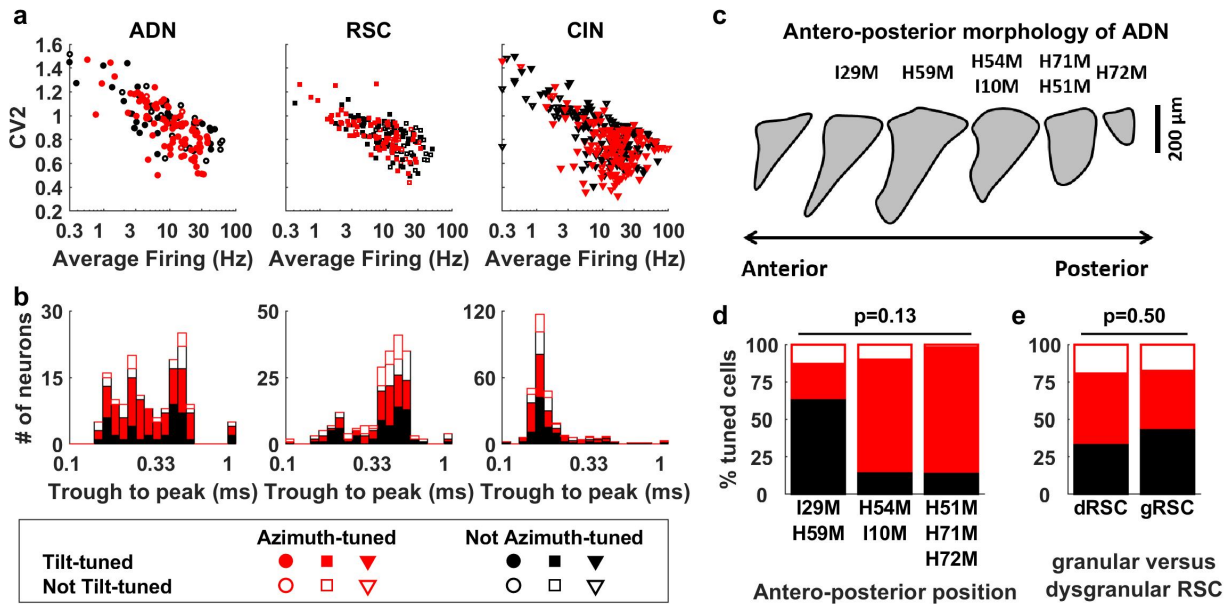
589 **Supplementary Figure 17: Comparison between the separable, multiplicative model of Fig. 4**  
 590 **and toroid topology<sup>9</sup>.**

591 **(a)** The toroid model is restricted to tilt movements in pitch, and assumes that azimuth  
 592 and pitch are independent, i.e. pitch movements don't change azimuth. Combination of pitch  
 593 and azimuth can be represented on the surface of a torus. Iso-pitch lines (green/blue/black color  
 594 code), that correspond to one pitch orientation and all possible azimuths, form horizontal circles.  
 595 Iso-azimuth lines (yellow/red color scale), that correspond to one azimuth angle and all possible  
 596 pitch tilts form vertical lines.

597 **(b)** Representation of the same iso-pitch and iso-azimuth lines in the 3D topology used in  
 598 this study, when azimuth is expressed in a TA frame. Each iso-azimuth line forms a D-shaped  
 599 curve that passes through UP, NU, UD and ND orientation, and each iso-pitch line forms a  
 600 horizontal line.

601 **(c)** When the diagram in (b) is looped upon itself to account for the circularity of azimuth  
 602 (note that this representation was not used outside of this figure because it distorts volumes),  
 603 the surface formed by iso-azimuth and iso-pitch lines adopts a toroidal topology identical to (a).  
 604 Thus, the 3D model used here is equivalent to the toroidal topology in (Finkelstein) if (1) tilt is  
 605 restricted to the pitch plane and (2) azimuth is expressed in the TA frame.

606



607

608 **Supplementary Figure 18: Firing properties and spatial distribution of responses.** To better  
 609 assess population responses in ADN, we included 3 additional animals (H51M, H54M and H59M)  
 610 in which cells could be classified using the same criteria as in other animals.

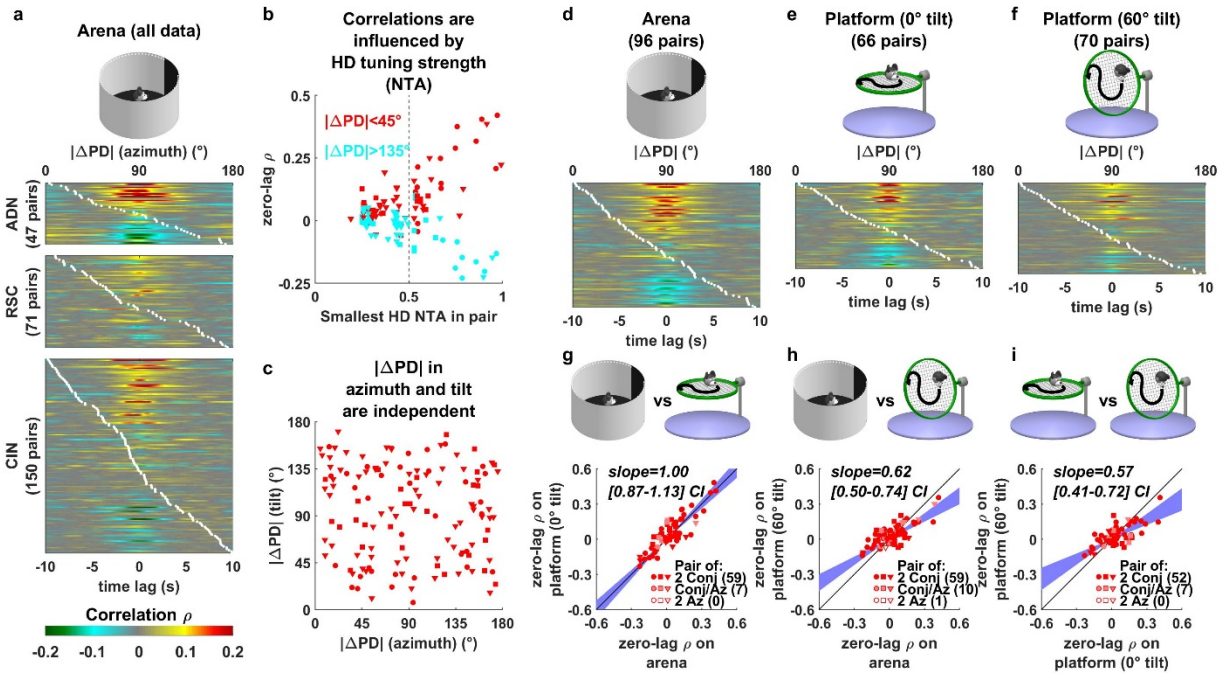
611 **(a)** Scatter plot of CV2 vs. average firing rate during freely moving in the arena. Median  
 612 firing rate: 10 Hz in ADN, 11 Hz in RSC, 13 Hz in CIN. Median CV2: 0.93 in ADN, 0.84 in RSC, 0.79  
 613 in CIN. CV2 varied significantly across areas (Kruskal-Wallis non-parametric ANOVA,  $p < 10^{-8}$ ), but  
 614 firing rate was similar ( $p=0.06$ ).

615 **(b)** Trough to peak duration of action potentials. Most (91%) cells in RSC have long trough  
 616 to peak spike duration ( $>0.33$ ms), whereas most (74%) cells in CIN have short spike duration.  
 617 About half (53%) of cells in the ADN have short spike duration; the proportions of conjunctive,  
 618 tilt-only, azimuth-only and non-responsive cells are 23%, 59%, 12% and 6% respectively amongst  
 619 ADN neurons with short spike duration and 30%, 49%, 14% and 7% amongst ADN neurons with  
 620 long spike duration: these proportions are similar across neurons with short- and long-duration  
 621 spikes (Chi square test,  $p = 0.77$ ,  $\chi^2=1.1$ , 3 dof). The CIN is a fiber bundle and neuronal activity  
 622 recorded therein is therefore expected to consist of axonal spikes, that can be recorded by  
 623 tetrodes<sup>12</sup> and typically exhibit small duration<sup>13</sup>. Note that most units recorded in the ADN also  
 624 had short-duration spikes. See Laurens et al (2019)<sup>14</sup> for further analyses of spiking activity in  
 625 these areas.

626           **(c,d)** Distribution of tilt- and azimuth-tuned cells along the antero-posterior axis of the  
627 ADN. (c) We identified the position of tetrode tracks in all animals by examining the cross-section  
628 of the ADN along successive brain sections. The anterior portion of the ADN has a triangular  
629 shape, which elongates into a narrow triangle before reaching a maximal cross-section size.  
630 Further along the posterior axis, the ADN decreases in size and adopts a rounder shape. The  
631 position of each animal is indicated. (d) Percentage of conjunctive, tilt-only and azimuth-only  
632 cells. The animals are pooled in 3 groups based on recording position corresponding to animals  
633 where recordings were at the most anterior, intermediate or most posterior position. The  
634 proportion of azimuth-tuned cells is lower in animals I29M and H59M, where tetrodes were  
635 placed in the anterior ADN over those recorded in intermediate and posterior AND (open/solid  
636 red bars, 36% versus 84%). However, the number of recorded animals is too low to establish  
637 whether the distribution of cell type depends significantly on recording position ( $p=0.13$ , Chi-  
638 square statistic, statistical significance evaluated by shuffling the recording position along  
639 animals).

640           **(e)** Percentage of conjunctive, tilt-only and azimuth-only cells in granular versus  
641 dysgranular RSC. We found no difference in the proportions of cells between these areas.

642



644

645 **Supplementary Fig. 19: The stability of the 1D attractor weakens when the head tilts.** When the

646 head is upright, the HD system is classically described as a 1D attractor where azimuth-tuned cells

647 with similar PD tend to fire together. Our findings question whether this attractor persists during

648 3D motion since (1) conjunctive cells with similar preferred azimuth direction but different

649 preferred tilt would fire at different tilt orientations, and (2) the tuning of azimuth-tuned cells

650 weaken when the head tilts. This suggests that the 1D attractor may weaken or disappear when

651 tilted. We tested this hypothesis by following the analysis in ref<sup>4</sup>. This study was based on the

652 cross-correlation between simultaneously recorded cells: HD cells with similar PD tend to fire

653 together whereas HD cells with opposite PD tend to be anti-correlated.

654 **(a)** Firing cross-correlograms (correlation as a function of time lag, lower abscissa) of all

655 pairs of azimuth-tuned cells recorded simultaneously in the arena. Within each brain region, cell

656 pairs are ordered based on the distance between their azimuth PD ( $|\Delta PD|$ , white, upper

657 abscissa). As expected, cells with similar PD (upper portion of the graphs) tend to fire

658 simultaneously (positive correlation at zero time lag, yellow/red colors) whereas cells with

659 opposite PD (lower parts of the graphs) rarely fire simultaneously (negative correlation,

660 cyan/green colors).



661           **(b)** Correlation at zero time lag, expressed as a function of the lowest HD tuning strength  
662 of both cells in the pair. As expected, pairs with similar (red) or opposite (cyan) PD are  
663 positively/negatively correlated when both cells exhibit strong HD tuning (e.g.  $NTA > 0.5$ ). In  
664 contrast, these correlations are close to zero when at least one cell in the pair is weakly tuned  
665 ( $NTA < 0.5$ ). In the following analyses, we exclude cells pairs where the lowest NTA is less than 0.5  
666 from panels (d-i) (although statistical analyses with all pairs included are mentioned in legend of  
667 panels g-i).

668           **(c)** Before proceeding further, we verify that cells with similar/opposite azimuth PD don't  
669 have similar/opposite tilt PD. Data shown is from 140/240 (58%) pairs of conjunctive cells where  
670 tilt tuning was recorded in the rotator. We find that differences are independent one from  
671 another (Spearman correlation rank = -0.01,  $p=0.6$ ).

672           **(d-f)** We now select pair of cells with strong HD tuning ( $NTA > 0.5$ , see panel b) and  
673 compare the correlations between cell pairs in the arena (d) and when walking on the platform  
674 in 3D. As a control, we separate recordings performed when the platform is horizontal (e) and  
675 when it is tilted by  $60^\circ$  (f). Note that we included all cells recorded on the platform, even if they  
676 didn't pass the criterion for uniform coverage of 3D space (see **Methods**, section Neuron  
677 selection and inclusion criteria, and **Table 1**), which is not important in the present analysis. Cells  
678 from all brain regions are pooled. As in (a), cells with similar/opposite PD exhibited  
679 positive/negative correlations at zero lag on all setups. Yet, further analysis revealed qualitative  
680 differences between these conditions.

681           **(g-i)** Comparison of the zero-lag correlations between conditions. Pairs are color-coded  
682 to indicate whether both cells are conjunctive (solid red), azimuth-only (open markers) or  
683 whether the pair contains one conjunctive and one azimuth-only cell (pink markers): note that  
684 most pairs are made of conjunctive cells. Zero-lag correlations were indistinguishable in the arena  
685 or on a horizontal platform (panel g; type II regression, slope not different from 1, bootstrap  
686 analysis). The slopes are similar if the inclusion criterion in panel b is lifted (0.97 [0.84 - 1.09] CI,  
687 0.64 [0.5 - 0.77] CI and 0.58 [0.45 - 0.73] CI in panels g, h and I respectively). In contrast, zero-lag  
688 were significantly reduced when the platform was tilted, compared to when exploring the arena


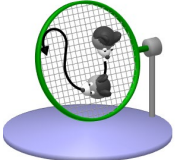
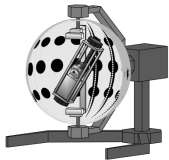

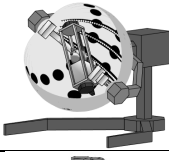
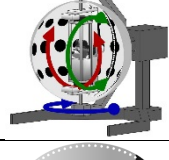
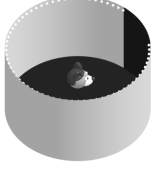
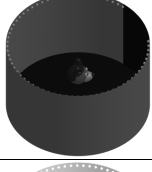
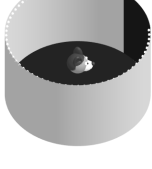
689 (h) or a horizontal platform (i) (bootstrap analysis, the confidence interval of the slopes don't  
690 overlap the confidence interval in (g)).

691         Conclusion: According to the neural attractor theory, azimuth-tuned cells with similar PD  
692 activate each other through reciprocal connections, which causes them to discharge together,  
693 whereas cells with opposite PD inhibit each other. This forms a 1D neural attractor where the  
694 population responses is always a packet of nearby active cells. Yet, most HD cells are in fact  
695 composite (g-i); thus, HD cells with similar preferred azimuth may have distinct preferred tilt (c).  
696 When the head tilts, we expect that such cells cease firing together, and this hypothesis is  
697 supported by the present analysis. We conclude that the HD system follows a 1D attractor  
698 dynamics when the head is upright, but not when the head tilts.

Animal name	H51M	H54M	H59M	H71M	H72M	I10M3	I29M	H65M	H68M	H69M	H74M	AA1	AA2	AA18	AA20	Total
Region	ADN	ADN	ADN	ADN	ADN	ADN	ADN	CIN	CIN	CIN	CIN	RSC	RSC	RSC	RSC	
<b>Total</b>	<b>14</b>	<b>37</b>	<b>42</b>	<b>35</b>	<b>13</b>	<b>6</b>	<b>15</b>	<b>72</b>	<b>137</b>	<b>61</b>	<b>27</b>	<b>53</b>	<b>124</b>	<b>8</b>	<b>29</b>	<b>580</b>
<i>Azimuth tuned</i>	6	30	12	33	9	6	4	34	68	29	17	26	58	0	20	304
<i>not Azimuth tuned</i>	8	7	30	2	4	0	11	38	69	32	10	27	66	8	9	276
<b>Experiment 2</b>																
<b>Platform</b>	<b>0</b>	<b>0</b>	<b>0</b>	<b>19</b>	<b>0</b>	<b>5</b>	<b>5</b>	<b>0</b>	<b>19</b>	<b>14</b>	<b>9</b>	<b>28</b>	<b>40</b>	<b>0</b>	<b>0</b>	<b>139</b>
<i>Conjunctive (Az&amp;Tilt)</i>	0	0	0	16	0	5	3	0	5	5	3	5	14	0	0	56
<i>Tilt-only</i>	0	0	0	0	0	0	1	0	6	3	4	6	16	0	0	36
<i>Azimuth-only</i>	0	0	0	1	0	0	0	0	1	2	1	9	5	0	0	19
<i>Not HD</i>	0	0	0	2	0	0	1	0	7	4	1	8	5	0	0	28
<i>Additional cells in Fig. S20</i>	0	0	0	1	0	1	0	0	20	7	7	0	19	0	0	55
<b>Experiment 3, D, T</b>																
<b>Rotator - in Light</b>	<b>14</b>	<b>37</b>	<b>40</b>	<b>30</b>	<b>13</b>	<b>3</b>	<b>14</b>	<b>72</b>	<b>137</b>	<b>59</b>	<b>19</b>	<b>53</b>	<b>114</b>	<b>8</b>	<b>27</b>	<b>549</b>
<i>Conjunctive (Az&amp;Tilt)</i>	6	27	6	30	8	2	3	28	47	25	11	14	37	0	17	222
<i>Tilt-only</i>	5	6	18	0	3	0	7	23	45	19	3	15	43	1	7	166
<i>Azimuth-only</i>	0	3	5	0	1	1	0	6	21	3	2	12	17	0	1	64
<i>Not HD</i>	3	1	11	0	1	0	4	15	24	12	3	12	17	7	2	97
<i>Rotator - in Darkness</i>	0 (0)	0 (0)	26 (13)	12 (12)	5 (4)	2 (1)	8 (6)	47 (33)	98 (68)	43 (32)	0 (0)	0 (0)	44 (30)	5 (1)	26 (23)	290 (210)
<i>Rotator - Tilted</i>	0 (0)	0 (0)	24 (12)	12 (12)	5 (3)	1 (1)	8 (6)	41 (26)	55 (38)	22 (16)	0 (0)	0 (0)	38 (27)	6 (1)	20 (18)	208 (148)
<b>Experiment 4: yaw, pitch, roll</b>	<b>0 (0)</b>	<b>0 (0)</b>	<b>0 (0)</b>	<b>0 (0)</b>	<b>0 (0)</b>	<b>0 (0)</b>	<b>0 (0)</b>	<b>40 (28)</b>	<b>18 (14)</b>	<b>11 (8)</b>	<b>0 (0)</b>	<b>0 (0)</b>	<b>0 (0)</b>	<b>0 (0)</b>	<b>0 (0)</b>	<b>69 (50)</b>

699

700 **Supplementary Table 1: Number of recorded cells and categories.** For each mouse (and each  
701 area), the table indicates the number of cells recorded during Experiment 1 (numbers in top row),  
702 2, 3 and 4), along with their categorization. The last column shows the total number of neurons  
703 tested for each experimental protocol. Grey lines and column: animals and cells that didn't pass  
704 the general inclusion criteria and are included only in specific Supplementary analyses. Animals  
705 H51M, H54M and H59M were recorded in an earlier version of the rotator (without orienting  
706 stripes) and are used only in Supplementary Fig. 18. These animals are not counted in the total  
707 number of cells. Some cells recorded on the platform were excluded as the animals didn't cover  
708 3D space well enough to compute 3D tuning curves, but were included in **Supplementary Fig. 19**.  
709

Experiment name	Illustration	Description	Goal
Experiment 1-L0		Free motion in arena.	Measure azimuth tuning using traditional method. Control for tuning stability (by comparing with Experiment 1-L1,2).
Experiment 2		Free motion on orientable platform.	Measure 3D tuning in freely moving animals at up to 60° tilt.
Experiment 3-L		3D tuning curve scanning in light.	Measure tuning uniformly in entire 3D space.
Experiment 3-D		3D tuning curve scanning in darkness.	Test that tilt tuning depends of gravity and not visual cues.
Experiment 3-T		3D tuning curve scanning in a tilted visual surround.	Test that tilt tuning depends of gravity and not visual cues.
Experiment 4		Rotations in yaw, pitch and roll (in light and darkness)	Test that 3D tuning is conserved during simple trajectories.
Experiment 1-L1		Free motion in arena.	Measure azimuth tuning using traditional method. Control for tuning stability (by comparing with Experiment 1-L0,2).
Experiment 1-D		Free motion in arena, in darkness.	Test that azimuth tuning is maintained in darkness.
Experiment 1-L2		Free motion in arena.	Measure azimuth tuning using traditional method. Control for tuning stability (by comparing with Experiment 1-L0,1).

711 **Supplementary References**

- 712 1. Lein, E. S. *et al.* Genome-wide atlas of gene expression in the adult mouse brain. *Nature* **445**,  
713 168–176 (2007).
- 714 2. Franklin, K. B. & Paxinos, G. *The mouse brain in stereotaxic coordinates*. vol. 3 (Academic  
715 press, New York, 2008).
- 716 3. Taube, J. S. The Head Direction Signal: Origins and Sensory-Motor Integration. *Annu. Rev.*  
717 *Neurosci.* **30**, 181–207 (2007).
- 718 4. Peyrache, A., Lacroix, M. M., Petersen, P. C. & Buzsáki, G. Internally organized mechanisms  
719 of the head direction sense. *Nat. Neurosci.* **18**, 569–575 (2015).
- 720 5. Yoder, R. M. & Taube, J. S. Head Direction Cell Activity in Mice: Robust Directional Signal  
721 Depends on Intact Otolith Organs. *J. Neurosci.* **29**, 1061–1076 (2009).
- 722 6. Park, E. H., Keeley, S., Savin, C., Ranck, J. B. & Fenton, A. A. How the Internally Organized  
723 Direction Sense Is Used to Navigate. *Neuron* **101**, 285-293.e5 (2019).
- 724 7. Jacob, P.-Y. *et al.* An independent, landmark-dominated head-direction signal in dysgranular  
725 retrosplenial cortex. *Nat. Neurosci.* **20**, 173–175 (2017).
- 726 8. Laurens, J. & Angelaki, D. E. The Brain Compass: A Perspective on How Self-Motion Updates  
727 the Head Direction Cell Attractor. *Neuron* **97**, 275–289 (2018).
- 728 9. Finkelstein, A. *et al.* Three-dimensional head-direction coding in the bat brain. *Nature* **517**,  
729 159–164 (2015).
- 730 10. Laurens, J. & Angelaki, D. E. A model-based reassessment of the three-dimensional tuning of  
731 head direction cells in rats. *J. Neurophysiol.* **122**, 1274–1287 (2019).
- 732 11. Shinder, M. E. & Taube, J. S. Three-dimensional tuning of head direction cells in rats. *J.*  
733 *Neurophysiol.* **121**, 4–37 (2019).
- 734 12. Robbins, A. A., Fox, S. E., Holmes, G. L., Scott, R. C. & Barry, J. M. Short duration waveforms  
735 recorded extracellularly from freely moving rats are representative of axonal activity. *Front.*  
736 *Neural Circuits* **7**, (2013).
- 737 13. Barry, J. M. Axonal activity in vivo: technical considerations and implications for the  
738 exploration of neural circuits in freely moving animals. *Front. Neurosci.* **9**, 153 (2015).

739 14. Laurens, J. *et al.* Multiplexed code of navigation variables in anterior limbic areas. *bioRxiv*  
740 684464 (2019) doi:10.1101/684464.  
741